TRIBHUVAN UNIVERSITY

INSTITUTE OF ENGINEERING

PULCHOWK CAMPUS

THESIS NO.:M-96-MSMDE-2023-2025

Experimental Study of Heat Transfer Enhancement in Concentric Heat Exchangers with Hybrid Nanoparticles

by

Laxmi Parajuli

A THESIS

SUBMITTED TO THE DEPARTMENT OF MECHANICAL AND AEROSPACE ENGINEERING IN PARTIAL FULFILLMENT OF THE REQUIREMENTS FOR THE DEGREE OF MASTER OF SCIENCE IN MECHANICAL SYSTEM DESIGN AND ENGINEERING

DEPARTMENT OF MECHANICAL AND AEROSPACE ENGINEERING

LALITPUR, NEPAL

December, 2025

COPYRIGHT

TRIBHUVAN UNIVERSITY

INSTITUTE OF ENGINEERING

PULCHOWK CAMPUS

DEPARTMENT OF MECHANICAL AND AEROSPACE ENGINEERING

The undersigned certify that they have read, and recommended to the Institute of Engineering for acceptance, a thesis entitled " **Experimental Study of Heat Transfer Enhancement in Concentric Heat Exchangers with Hybrid Nanoparticles** " submitted by Laxmi Parajuli in partial fulfillment of the requirements for the degree of Master of Science in Mechanical System Design and Engineering.

Supervisor, Dr. Surya Pd. Adhikari
Associate Professor
Department Of Mechanical and Aerospace Engineering

Supervisor, Navin K Jha
Assistant Professor
Department Of Mechanical and Aerospace Engineering

External Examiner, Dr. Daniel Tuladhar
Professor
Department of Mechanical Engineering,
School of Engineering , KU

Tribhuvan University
Institute of Engineering
Department of Mechanical and Aerospace Engineering
Pulchowk Campus

Committee Chairperson, Dr. Sudip Bhattrai
Assistant Professor/Head of Department
Department Of Mechanical and Aerospace Engineering

Date:1st December, 2025

ABSTRACT

Nanofluids and turbulators have attracted considerable attention as they enhance heat transfer. Experimental studies were conducted utilizing a helical coil turbulator along with CuO-Al_2O_3-water hybrid nanofluid and CuO-water nanofluids on a counter flow concentric heat exchanger. Nanoparticles of CuO and Al_2O_3 were produced via the sol-gel method, while a two-step process was employed to create the nanofluids. A concentric heat exchanger was designed, in which a hot fluid at 70º C and a cold fluid at 25º C were circulated. Experimental results indicate that adding CuO nanoparticles and CuO-Al_2O_3 hybrid nanoparticles to water improved heat transfer, and a 12 mm turbulator enhanced heat transfer more effectively than 18 mm turbulator. The maximum overall heat transfer coefficients reached 61.16 % for CuO-Al_2O_3 (75:25) hybrid-nanofluid with a 12 mm turbulator at 10.4 LPM, in comparison to CuO-Al_2O_3 (75:25) hybrid-nanofluid without a turbulator.

ACKNOWLEDGMENTS

I wish to convey my heartfelt thanks to Associate Professor Surya Prasad Adhikari, PhD for guiding my thesis research. I sincerely thank Assistant Professor Navin K Jha for overseeing my thesis work. Without their essential guidance, this research work would not have been completed.

I would like to express my gratitude to Dr. Khem Gyanwali, Principal of Thapathali Campus, IOE, for granting me permission to utilize the Workshop facilities for my research. Additionally, I want to express my gratitude to Assistant Professor Lochan Kendra Devkota for consistently assisting with fabrication and experimental tasks at Thapathali Campus.

I am also very thankful to Er. Sudeep Shah for helping me with the experimental setup.

I want to express my gratitude to everyone who has assisted me in this thesis work in different ways.

Table of Contents

LIST OF FIGURES

LIST OF TABLES

LIST OF ABBREVIATIONS AND ACRONYMS

A	Total heat transfer area
kf	Thermal Conductivity of base fluid
khnf	Thermal conductivity of hybrid nanofluids
K1	Thermal conductivity of CuO nanoparticles
K2	Thermal Conductivity of Al_2O_3 nanoparticles
Q	Total Heat transfer
q	Flow rate
Re	Reynold number
T	Temperature
T_{C1}	cold fluid's temperature before heat transfer
T_{C2}	cold fluid's temperature after heat transfer
T_{h1}	Hot fluid's temperature before heat transfer
T_{h2}	Hot fluid's temperature after heat transfer
U	Overall heat transfer coefficient
μf	Dynamic viscosity of the fluid
μhnf	viscosity of hybrid nanofluid
ρf	Density of the fluid
ρhnf	density of hybrid nanofluid
ϕ	volume concentrations of hybrid nanoparticles
ϕ_1	volume concentrations of CuO nanoparticles
ϕ_2	volume concentrations of Al_2O_3 nanoparticles
(ρ)CuO	density of CuO nanoparticles
(ρ)Al_2O_3	density of Al_2O_3 nanoparticles
(Cp)f	Specific Heat Capacity of base fluid
(Cp)Al_2O_3	Specific Heat Capacity of Al_2O_3 nanoparticles
(Cp)CuO	Specific Heat Capacity of CuO nanoparticles
Cphnf	Specific Heat Capacity of hybrid nanofluid
N	an integer,
λ	wavelength of the X-rays
d	distance between the planes that causes the diffraction
θ	The Bragg angle
D	crystalline size
K	crystalline shape factor
β	(FWHM) of the X-ray diffraction peak

CHAPTER ONE: INTRODUCTION

1.1 Background

The world is expanding quickly, made possible by both traditional and renewable energy sources. Energy is essential for technological advancement, yet conventional energy sources are decreasing at an alarming rate. In today's world, with increasing energy costs, rising environmental pollution, and restrictions on fossil fuel use, optimizing energy efficiency has become critical (Shahmohammadi and Beiki, 2016).

A heat exchanger is an apparatus that transfers thermal energy between two liquids without permitting them to mix. Heat exchangers play a crucial role in numerous industrial applications, such as power generation, chemical processing, and HVAC systems. Heat exchangers play a crucial role in various machines due to their function of heating and cooling fluids based on the application. There is a range of heat exchangers utilized in various applications. Shell and tube heat exchangers consist of tubes enclosed within a shell and are used in power generation, chemical processes, and petroleum refineries. Plate Heat Exchangers are thin, corrugated plates that are utilized in HVAC systems, food processing, and the dairy industry. Plate and Frame Heat Exchangers have plates held together in a frame, making them simple to disassemble for cleaning. Regenerative Heat Exchangers momentarily store heat in a medium before transferring it to a cool fluid.

Concentric heat exchangers, also referred to as double-pipe heat exchangers, feature one pipe encased within another and are well-known for their easy design, maintenance convenience, and effectiveness. As the demand for greater efficiency and more compact designs grows, the current heat transfer methods in concentric heat exchangers are being pushed to their limits. This has resulted in the creation of new heat transfer methods aimed at enhancing the thermal efficiency of these systems.

The performance of a heat exchanger can be improved by refining design parameters, employing fluids with good thermal conductivities, and more. A promising technique for boosting the efficiency of heat exchangers is the use of hybrid nanofluids. Nanofluids have the potential to enhance the thermal efficiency of heat exchanger systems. (Akyürek et al., 2018).

Choi and Eastman, (1995) States that nanofluids are designed fluids made by spreading nano-sized (1-100 nm) particles of metals, nonmetals, or oxides into a base or

conventional fluid. The addition of high-thermal conductivity nanoparticles considerably improves the base fluid's thermal conductivity and heat transmission capabilities.

Another popular way for improving heat exchanger performance and reducing energy consumption, which leads to pollution management, is to employ a turbulator. A turbulator is a device or feature used in a fluid flow system to generate turbulence. Turbulators are frequently used in heat exchangers to disrupt the fluid's laminar flow, enhancing heat transfer. By generating turbulence, they enhance fluid mixing and consequently increase thermal interaction between the fluid and the heat exchange surface. To ensure a steady heat transfer area in heat exchangers and enhance heat transfer efficiency, various turbulators like ribs, baffles, delta winglets, louvered, and perforated designs are applied to the fin surfaces. Nonetheless, the pressure loss is considerable and differs based on the turbulator type and flow conditions (Çelik and Erbay, 2021). Turbulators are added to the flow to regenerate the boundary layer, increase the heat transfer surface area, and enhance heat transmission by boosting turbulence or fast fluid mixing (Promvonge, 2008).

1.2 Statement of the problems

Increased energy usage immediately correlates with higher operational expenses, which is a major concern in today's competitive industrial world. In addition to the economic ramifications, excessive usage of traditional energy sources has serious environmental impacts such as: air pollution and ozone depletion. Furthermore, energy loss through the system due to less effective heat exchanger decreases the efficiency of the machine, overheating reduces the lifecycle of the material and is the cause of component failure.

These ecological effects, together with efficiency and expense factors, emphasize the enhancement of the system's component, thereby helping to decrease energy usage. An efficient way to accomplish this is through the optimization of heat exchangers. Heat exchangers are essential components of many industrial processes and play an important role in thermal energy management. Heat exchangers in cooling applications must efficiently extract heat from fluids inside the system in order to improve the overall system efficiency. Enhancing the performance of these heat exchangers can save a significant amount of energy.

By carefully examining the mechanisms responsible for enhancing heat transfer and their influence on overall efficiency, this study aims to offer meaningful guidance for the

design and improvement of concentric heat exchanger systems. In this work, several parameters of the concentric heat exchanger will be modified to evaluate their effects. For example, adjusting the dimensions of turbulators and adding nanoparticles to traditional fluids will be investigated. The results are expected to support the creation of more compact and efficient heat exchangers, helping address increasing energy requirements and environmental issues in current industrial applications.

1.3 Objective

1.3.1. Main Objectives

- To perform the synergistic effects of hybrid nanofluids (Blends of CuO, Al_2O_3 and water) and turbulator size variations on the thermal performance of concentric heat exchangers.

1.3.2. Specific Objective

- To synthesize and blend hybrid nanofluids in three different proportion
- To analyze the pressure and temperature contour using CFD
- To calculate heat transfer for different proportion of hybrid nanofluid along with various turbulator
- To calculate pressure loss for different proportion of hybrid nanofluid along with various turbulator

1.4 Scope of the work

- The correct fraction of hybrid nanofluids may be found for future applications, ensuring their effectiveness in improving heat transfer efficiency.
- Energy consumption can be reduced by optimizing concentration of nanoparticles resulting in more efficient heat exchanger systems.
- An ideal design for concentric heat exchangers can be created and optimized for commercial manufacturing, providing a high-performance solution for industrial applications.

1.5 Challenges of the work

- Measuring the thermal characteristics of hybrid nanofluids is difficult in our country because of a lack of an equipment and experience, and outsourcing these experiments might be prohibitively expensive.

- Hybrid nanofluid production and mixing can be difficult and time-consuming procedures that frequently necessitate the use of specialized techniques and equipment.
- The high cost of nanoparticles adds to the financial burden of research.
- Setting up tests can be time-consuming and difficult, requiring cautious planning, precise execution, and lengthy testing to assure dependable and accurate results.
- Accurately analyzing and minimizing energy consumption may involve complex simulations and real-world testing, adding to the research's complexity and resource demands.

1.6 **Limitations of Research**

All research has some constraints, and some of the constraints of this study are outlined below.

- Nanoparticle Type: In this study, two specific nanoparticles: Al_2O_3 and CuO are considered to prepare hybrid nanoparticles. Other various combinations can be made.
- Concentrations: The study focuses exclusively on concentrations of hybrid nanoparticles of 0.01% by volume. The proportion of CuO and Al_2O_3 are; 25:75, 50:50 and 75:25 only.
- Experimental Conditions: Particular flow rates and temperature ranges were used for the experiments. This study did not examine how changes in these parameters would affect the pressure drop and overall heat transfer coefficient.
- Long-term Stability and Fouling: Neither the possible fouling effects on the heat exchanger surfaces nor the long-term stability of the nanoparticles in water were evaluated. These elements may have a major effect on the maintenance needs and practical use of heat exchangers.
- Limitations of Numerical Simulations: In order to mimic the flow and heat transfer properties, the numerical simulations made a number of assumptions and simplifications.These presumptions may not adequately account for the complexities of practical applications, which could have an impact on the findings accurate data as well as validating the experimental findings.

- Environmental Considerations: The study did not investigate how employing hybrid nanoparticles in water of industrial heat exchangers will affect the environment.

CHAPTER TWO: LITERATURE REVIEW

A heat exchanger conveys thermal energy from a fluid with high temperature to one with low temperature as both fluids flow through it. Flowing fluids exchange heat in several industrial processes, including air intercoolers and preheaters, steam plant condensers and boilers, refrigerator evaporators, and more (Eckert and Drake, 1987).

Turbulators or baffles are used to increase turbulence within a heat exchanger. Promvonge, (2008) shows that employing coiled square wire turbulators leads to a notable enhancement in heat transfer and friction loss compared to a smooth wall tube. For both circular and square wire coils, the Nusselt number increases with rising Reynolds numbers and decreasing pitch. In the same conditions, the square coiled wire transfers more heat than the circular wire.

Azmi et al.,(2014) examined turbulent heat transfer and friction factors of water-based TiO_2 and SiO_2 nanofluids within a circular tube subjected to a constant heat flux. Nanoparticles measuring 50 nm (TiO_2) and 22 nm (SiO_2) were evaluated at concentrations reaching 3% and Reynolds numbers ranging from 5000 to 25,000. TiO_2 exhibited greater rises in viscosity and thermal conductivity compared to SiO_2. The increase in nanoparticle density led to a rise in pressure drop.

Rajendra et al., (2016) introduced a method to boost the performance of shell-and-tube heat exchangers by expanding the effective heat-transfer area using textured or grooved tube surfaces. The approach also includes the use of internal inserts designed to enhance turbulence inside the tubes, further improving heat-transfer efficiency.

Wanatasanappan et al., (2020) examined the effect of nanoparticle proportion and temperature of nanofluid on the thermal conductivity of Al_2O_3-Cuo/water-EG hybrid nanofluid. Al_2O_3-CuO hybrid nanofluid demonstrates superior thermal efficiency compared to the base fluid (water-EG) during forced convection heat transfer.

Zhang et al., (2021) created a hybrid Al_2O_3–CuO/water nanofluid and assessed its turbulent flow and heat transfer properties in a circular pipe.Experiments assessed the heat transfer coefficient and pressure loss at nanofluid concentrations ranging from 0.5% to 3% across different Reynolds numbers.Results show that employing hybrid nanofluids can notably enhance heat transfer efficiency and affects flow resistance as well.

Both turbulent flow and nanofluids greatly improve convective heat transfer, with the extent of enhancement affected by Reynolds number, flow structure, and the

incorporation of devices to promote turbulence, like helical coil inserts. Although these techniques enhance heat transfer rates, they simultaneously raise pressure drop, necessitating careful design compromises. Current research shows that nanofluids in turbulent flow tubes can enhance heat exchanger effectiveness, yet most studies concentrate on individual nanofluids or constant concentrations.

There is a lack of studies on hybrid nanofluids with different nanoparticle ratios in turbulated tubes, especially concerning the joint impacts on heat transfer improvement and pressure drop. This emphasizes the necessity for systematic research on ideal nanoparticle ratios in hybrid nanofluids to enhance thermal efficiency while managing flow resistance.

2.1 Method of increasing effectiveness of Heat Exchanger

2.1.1 Heat Exchanger with Turbulator

Heat exchanger effectiveness can be improved using active or passive approaches. Active methods contribute energy to the fluid or equipment, whereas passive methods promote heat transfer without adding energy. Passive approaches include covering or modifying the heat transmission surface, as well as generating projecting sections of rough surfaces. Surface area expansions are utilized to boost heat transfer rates, however attachable turbulators are getting more attention due to manufacturing challenges, continual director fins, and maintenance issues (Karakaya & Durmuş 2013).

Alkam and Al-Nimr, (1999) presents an innovative method for enhancing the thermal efficiency of a standard concentric tube heat exchanger by positioning porous materials on either side of the inner tube wall, thereby boosting the convective heat transfer coefficient between the tube walls and the fluid. They also study assessed the efficacy of this approach for parallel and counter flow configurations, particularly at high heat capacity ratios.

Nalavade et al., (2019) examines the friction coefficient and forced convection heat transfer characteristics of air movement within a heated tube fitted with advanced flow divider type turbulators. They conducted simulation experiments for turbulent flow conditions with Reynolds numbers between 7000 and 21000 and discovered that the turbulators induce extra turbulence along the wall of the tube, thereby disturbing the thermal boundary layer. They concluded that heat transmission rate, friction factor, and thermal enhancement factor all rose as the pitch to diameter ratio decreased.

Shah et al., (2021) uses numerical simulation to model hybrid nanofluid turbulent motion via a pipe with a constant heat flux. A helical turbulator generates secondary flow, and FVM is used to solve flow and temperature equations. Entropy optimization is utilized to examine forced convective features. The results reveal that fluid temperature declines, velocity increases with Reynolds number, thermal irreversibility reduces, and frictional irreversibility increases with increased turbulence. Reduced pitch ratio improves fluid velocity while decreasing fluid temperature.

Wollele et al., (2022) evaluated the improvement of heat transfer for an Al_2O_3–Cu/water hybrid nanofluid in a circular duct, comparing scenarios with and without the inclusion of twisted tape inserts.With a Reynolds number of 20,000, the presence of the twisted tape enhances fluid mixing, leading to a temperature increase of approximately 1–1.75% in comparison to the smooth tube.The Nusselt number for the twisted tape setup is 1.5–2.0% greater than that of the smooth tube. In general, the use of twisted tape enhances the performance evaluation metric by approximately 1.01 times compared to the setup without inserts.

2.1.2 Heat Exchanger with nanofluids

Shabi et al., (2024) performed an experimental study on shell and helical coiled heat exchangers utilizing Al_2O_3 nanoparticles. The research revealed that nanoparticles greatly enhanced the heat transfer coefficient within the helically coiled tube.

Shahmohammadi & Beiki, (2016) conducted a numerical study of Al_2O_3 water nanofluids in a shell and tube heat exchanger. The research found that mass flow rate and baffle quantity led to an increase in heat transfer and pressure drop.

Ghashim, (2021) conducted CFD simulations on water mixing with nanoparticles in pipes under uniform heat flux. The addition of Al_2O_3-Cu particles restrict thermal boundary layer growth, increasing bulk temperature and heat transfer coefficient. The Nusselt number (Nu) ratio of hybrid nanofluid rises with the volume concentration of nanoparticles.

2.2 Synthesis of Nanoparticles

Nanoparticles can be developed utilizing a variety of ways, including physical, chemical and procedures. Here are some popular methods in each category:

2.2.1 Physical methods:

a) **Ball Milling:** Mechanical grinding of bulk materials produces nanoparticles. Benefits: Simple, scalable, and cost-effective.

b) **Laser ablation**: Laser ablation involves using laser pulses to remove material from a target in liquid or gas. The major advantages are: High purity nanoparticles, with control over particle size.

c) Physical Vapor Deposition (PVD): PVD is a process that involves vaporizing material in a vacuum and condensing it on a cool substrate. The major advantages are to create high-purity nanoparticles ideal for thin films.

2.2.2 Chemical Methods

a) Chemical Reduction: Metal salts are reduced in solution using reducing agents (such as sodium borohydride). Advantages: Simple and extensively used, with control over particle size and shape.

b) Sol-Gel method: The process involves hydrolysis and polycondensation of metal alkoxides to generate a gel, which is subsequently dried and calcined. A sol is a colloidal dispersion with extremely small particles that rely on surface charges and Van der Waals forces rather than gravity. When a sol's solvent evaporates, particles or ions form into a continuous network to produce a gel. This process provides good composition and purity control, making it excellent for oxide applications.

c) Co-precipitation: The process involves the simultaneous precipitation of several precursors in solution. Advantages: Simple, cost-effective, and scalable.

2.3 **Nanofluid Preparation**

Nanofluids are categorized into single or mono-nanofluids and hybrid nanofluids. A mono-nanofluid contains just one kind of nanoparticle within the base fluid. In contrast, hybrid nanofluids combine several nanoparticles with the base fluid(Modi et al., 2023). The stability of nanofluid depends on the selection of its preparation method, which affects its thermophysical properties, and the two most common methods are Two-step and One-step (Awais et al., 2021). Nanofluids, produced through one-step and two-step methods, are stable and highly conductive but face issues with nanoparticle agglomeration, which is a crucial issue (Said et al., 2022).

The two-step process, which is cost-effective for large-scale production, uses nanomaterials such nanoparticles, nanofibers, and nanotubes to make dry powders, is frequently employed to prepare nanofluids. Next, using a variety of methods such as high-shear mixing, ball milling, homogenizing, magnetic force agitation, and ultrasonic agitation, the nanosized powder is distributed into a base fluid (Rathodiya and Vishnoi, 2017).

The one-step method combines nanoparticle synthesis with suspension in base fluid or nanofluid preparation in a single process. The nanofluid is created in one step through methods like direct evaporation, physical vapor deposition, liquid chemical direct evaporation, and others. The benefits include the capacity to manage the size and form of nanoparticles, avoid the need of stabilizers, achieve very good stability, nanofluid homogeneity, and prevent nanoparticle aggregation (Pordanjani et al., 2021 : Modi et al., 2023) .

Nanofluids increase temperature difference due to Brownian motion and agglomeration. Dispersing nanoparticles in base fluids leads to Brownian motion, increasing thermal conductivity and heat transfer. As nanofluids pass through a cross-section, they form micro particles, forming percolation paths and increasing thermal conductivity. The level of aggregation depends on the synthesis method and purity of the nanoparticles. Green synthesis is a promising cost-effective and eco-friendly method for nanofluids, with potential applications in engineering (Narayanan and Rakesh, 2019).

Using surfactants is a typical method to improve the stability of nanoparticles in fluids. But, particularly for high-temperature applications, the surfactants' ability to function at high temperatures is also crucial (Rathodiya and Vishnoi, 2017).

The sol-gel method is a chemical approach for creating nanostructures, especially metal oxide nanoparticles. This process includes dissolving a precursor in water or alcohol, heating and mixing, and transforming it into a gel via hydrolysis/alcoholysis. The gel is subsequently dried, ground into powder, and then calcined. This economical approach provides excellent control over chemical composition and is applicable in ceramics and thin metal oxide layers.The properties of the dried gel depend on the drying method (Bokov et al., 2021).

Numerous approaches for blending nanoparticles to obtain homogenous dispersion in a matrix or creating hybrid nanoparticles are mentioned in the different literature. Some methods are given below:

a) **Ball milling**: It is the process of mechanically grinding nanoparticles with a matrix material utilizing revolving drums.
b) **High-Shear Mixing**: This process involves using high-speed mixers to combine nanoparticles into a matrix.
c) **In situ synthesis**: It involves producing nanoparticles immediately in the presence of a matrix material.
d) **Magnetic Stirring:** The process of dispersing nanoparticles in a liquid media involves using a magnetic stirrer.

2.4 **Thermophysical property of nanofluid**

The fundamental characteristics of nanofluids that dictate their flow behavior and heat transfer are known as their thermophysical properties. These characteristics which are crucial for improving heat transfer processes include density, specific heat, viscosity, and thermal conductivity.

2.4.1 Viscosity

The presence of nanoparticles makes the fluid more viscous. Nanoparticles can accumulate and restrict fluid flow.

Viscosity is the most important parameter that plays a crucial role in transporting nanofluids and also decides the pumping power. So, it is necessary to study the effect of the concentration of hybrid nanofluids on the viscosity and base fluid (Shaik et al., 2024).

Brinkman model: $\mu nf = \mu bf \frac{1}{(1-\emptyset)^2}$ Equation 2. 1

Batchelor model: (Vajjha et al., 2010)

$\mu nf = \mu bf\ (1 + 2.5 * \emptyset + 6.2 * \emptyset^2)$ Equation 2. 2

Shaik et al., (2024) concluded that the Brinkman model, with an R2 value of 0.97868, and the Batchelor model, with an R2 value of 0.97872, well fitted water-based hybrid nanofluid after conducting an experimental analysis and comparing the results with various theoretical models.

2.4.2 Density

Incorporating nanoparticles causes fluid density to increase due to their higher density than the base fluid.

The density of the nanofluid (ρnf) is calculated using the physical mixture rule, taking densities of the base fluid (ρf) and nanoparticles (ρnp) and volume concentration ϕ.(Alosious et al., 2017)

$$(\rho)nf = Ø\,(\rho)np + (1 - Ø)(\rho)f \quad \text{Equation 2. 3}$$

$$Ø = \frac{wnp/\rho np) \times 100}{\left[\left(\frac{wnp}{\rho np}\right) + \left(\frac{wbf}{\rho bf}\right)\right]} \quad \text{Equation 2. 4}$$

The hybrid nanofluid's density is calculated in relation to the mass fraction of nanoparticles.(Ho et al., 2010)

$$(\rho)hnf = Ø1(\rho)s1 + Ø2(\rho)s2 + (1 - Ø)(\rho)f \quad \text{Equation 2. 5}$$

2.4.3 Specific Heat Capacity

When evaluating the thermal performance of heat exchangers, specific heat is a crucial thermophysical property.

With the assumption of thermal equilibrium between the base fluid and nanoparticles, the physical mixture rule can be used to obtain the equations for specific heat, which provide a good agreement with the experimental works (Xuan and Roetzel, n.d.).

$$(\rho cp)nf = (1 - Ø)(\rho cp)f + Ø(\rho cp)s \quad \text{Equation 2. 6}$$

The specific heat of hybrid nanofluids is expressed as (Ho et al., 2010; Shaik et al., 2024)

$$(\rho Cp)hnf = Ø1(\rho Cp)s1 + Ø2(\rho Cp)s2 + (1 - Ø)(\rho Cp)f \quad \text{Equation 2. 7}$$

The specific heat capacity of the base fluid (water), hybrid nanofluid, and nanoparticles 1 and 2 are denoted by the letters Cpf, Cphnf, Cps1, Cps2. The densities of the base fluid, hybrid nanofluid, and nanoparticles 1 and 2 are denoted by ρf, ρhnf, ρs1 and ρs2 respectively. Ø, Ø1, and Ø2 represent the volume concentrations of base fluid and nanoparticles 1 and 2 respectively.

2.4.4 Thermal Conductivity

Incorporating nanoparticles improves the thermal conductivity of the base fluid because of the high surface area to volume ratio, leading to more effective energy transfer .

The capability of a substance to transfer or conduct heat is referred to as thermal conductivity .In order to utilize dispersed fluids as a working medium to enhance heat transfer performance, better selection of particles, i.e., selecting particles that have higher thermal conductivity and larger size, is a crucial point (Pak & Cho, 1998).

The thermal conductivity can be determined via following equation (Hassaan, 2024)

$$\frac{knf}{kw} = \frac{\frac{(Ø1k1 + Ø2k2)}{Ø} + 2kf + 2\,(Ø1k1 + Ø\,2k2) - 2Ø\,kf}{\frac{Φ1k1 + Ø\,2k2}{Ø} + 2kf + 2\,(Ø1k1 + Ø\,2k2) + Ø\,kf} \qquad \text{Equation 2. 8}$$

2.5 **Nanoparticle Characterization Technique**

X-Ray Diffraction (XRD) is an important characterization technique for nanoparticles. This technique is used for phase identification, purity, crystalline size etc. XRD is a non-invasive and non-destructive technique for analyzing crystalline phases, polymeric structures, and material properties.In a mixture of substances, each one generates its own pattern independently of the others, and every crystalline substance always produces the same pattern (Saraugi, 2024).

2.5.1 Bragg's law

When the incoming rays strike the sample, they produce constructive interference and a diffracted ray when the conditions satisfy Bragg's law. The incident beam, diffracted beam is shown in Figure 2.1 (Saraugi, 2024) .

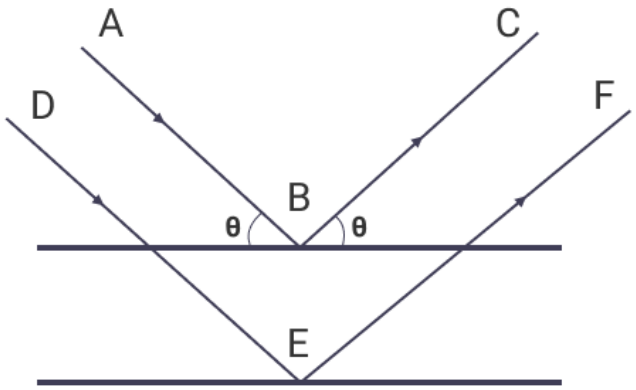

Figure 2. 1: Bragg's laws incident beam, diffracted beam

Bragg's law indicates that when X-rays hit a crystal surface, the angle at which they strike (θ) is equal to the angle of scattering (θ). Constructive interference happens when the path difference (d) is equal to a specified number (n) of wavelengths (λ). XRD (X-ray

diffraction) characterizes and identifies a crystal by utilizing its inter-planar spacing, known as d-spacing.

$N\lambda=2d\ Sin\theta$ Equation 2. 9

Where N represents an integer,

λ represents the wavelength of the X-rays,

d represents the separation between the planes that leads to the diffraction,

And θ represents the diffraction angle.

2.5.2 Calculation of Particle size using XRD graph

In X-ray diffraction and crystallography, the Scherrer equation is a mathematical expression that relates the dimensions of sub-micrometer crystallites in a substance to the widening of a peak in a diffraction pattern. The Scherrer equation is limited to nanoscale crystallites, or more accurately, the size of the coherently scattering domain, which may be less than the size of the crystallite. The Scherrer equation provides a lower bound for the size of the coherently scattering domain, commonly known as the crystallite size for clarity. This occurs because, aside from instrumental effects and crystallite size, several other factors can affect the width of a diffraction peak; the primary ones are usually inhomogeneous strain and defects in the crystal lattice.

The Scherrer equation is written as:

$D=k\lambda/(\beta\ Cos\theta)$ Equation 2. 10

Where,

D= crystalline size

K= crystalline shape factor (Usually taken 0.94)

λ= X-ray wavelength =0.154

β= The full-width at half-maximum (FWHM) of the X-ray diffraction peak, expressed in radians.

θ= The Bragg angle, which is equals half the peak center angle (2θ)

2.6 Overall Heat Transfer Coefficient (U)

Following formula was used for the analysis of heat transfer.

$$U = \frac{Q}{A*LMTD}$$ Equation 2. 11

$$Q\ hot\ = q * (\rho Cp)f * (Th1 - Th2)$$ Equation 2. 12

$$Q\ Cold\ = q * (\rho Cp)hnf * (Tc2 - Tc1)$$ Equation 2. 13

$$Q = \frac{Qhot+Qcold}{2}$$ Equation 2. 14

$$LMTD = \frac{(Th1-Tc2)-(Th2-Tc1)}{ln(Th1-Tc2)/(Th2-Tc1)}$$ Equation 2. 15

$$A\ = Pi * Di * L$$ Equation 2. 16

Where, Th1, Th2, Tc1, Tc2 is inlet and outlet temperatures of hot fluid and cold fluid respectively. A is surface area of inner tube and LMTD represents Logarithmic mean temperature difference (K).

2.7 Governing Equations for CFD analysis

The analysis of heat exchangers using Computational Fluid Dynamics (CFD) relies on the numerical resolution of a series of conservation equations that characterize fluid motion and heat exchange. These equations are based on essential physical principles, such as the conservation of mass, momentum, and energy. In most engineering contexts, the working fluid is considered Newtonian, and the flow can either be laminar or turbulent based on the operating Reynolds number. Numerical solutions are generally obtained through the finite volume method, which transforms the governing equations into a discretized algebraic format appropriate for computational resolution.

2.7.1 Conservation of mass

The principle of mass conservation, or continuity equation, guarantees that mass is not created or eliminated within the control volume. For a fluid that cannot be compressed, which is typically assumed in heat exchanger simulations, the continuity equation is formulated as:

$$\nabla.(\rho u) = 0$$ Equation 2. 17

This equation ensures that the mass flow rate that enters and exits a control volume remains unchanged .

2.7.2 Conservation of momentum

The preservation of momentum refers to the transmission of linear momentum in the flow and is mathematically expressed by the Navier–Stokes equations. These equations

consider the forces of inertia, pressure, viscosity, and body acting on the fluid. In its incompressible form, the momentum equation is expressed as:

$$\rho\left(\frac{\delta u}{\delta t} + u.\nabla u\right) = -\nabla p + \mu\nabla^2 u + \rho g \qquad \text{Equation 2. 18}$$

Flows in heat exchangers are typically turbulent; hence, the Reynolds-averaged Navier–Stokes (RANS) equations are frequently employed to simulate turbulence models.

2.7.3 Conservation of Energy

The energy equation explains the movement of thermal energy through convection and conduction. For incompressible flow where thermophysical properties are constant, the energy equation can be expressed as:

$$\rho c_p\left(\frac{\delta T}{\delta t} + u.\nabla T\right) = k\nabla^2 T + \varphi \qquad \text{Equation 2. 19}$$

Where φ represents viscous dissipation, which is typically insignificant in low-speed flows. This equation dictates the forecasting of temperature distributions, heat transfer rates, and total thermal efficiency of the heat exchanger.

2.7.4 Turbulence Modeling

Turbulence improves momentum and heat transfer processes; therefore, modeling turbulence is essential for heat exchanger analysis in CFD. The RANS formulations add extra unknowns, necessitating closure via turbulence models. A commonly utilized model is the standard k−ε model, which addresses two extra transport equations:

Turbulent kinetic energy:

$$\frac{\delta(\rho k)}{\delta t} + \nabla.(\rho k u) = \nabla.\left[\left(\mu + \frac{\mu_t}{\sigma_k}\right)\nabla k\right] + G_k - \rho\epsilon \qquad \text{Equation 2. 20}$$

Turbulent dissipation rate:

$$\frac{\delta(\rho\epsilon)}{\delta t} + \nabla.(\rho\epsilon u) = \nabla.\left[\left(\mu + \frac{\mu_t}{\sigma_\epsilon}\right)\nabla\epsilon\right] + C_{1\epsilon}\frac{\epsilon}{k}G_k - C_{2\epsilon}\rho\epsilon \qquad \text{Equation 2. 21}$$

These models are frequently utilized in heat exchanger simulations because of their acceptable accuracy and computational effectiveness.

2.7.5 Solid Region Heat Conduction

In heat exchanger uses, heat is moved not just through the fluid areas but also through the solid walls or fins. Heat transfer within the solid area is controlled by:

$$\rho_s c_{p,s} \frac{\delta T}{\delta t} = k_s \nabla^2 T$$ Equation 2. 22

The coupling between fluid and solid areas is established by maintaining continuity of temperature and heat flux at the interface.

2.7.6 Fluid-Solid Interaction

At the interface between the fluid and solid, two physical conditions need to be met:

Continuity of temperature:

$$T_f = T_s$$ Equation 2. 23

Continuity of heat flux:

$$K_f \frac{\delta T_f}{\delta n} = K_s \frac{\delta T_s}{\delta n}$$ Equation 2. 24

These interactions allow CFD solvers to accurately forecast heat transfer through solid walls.

CHAPTER THREE: METHODOLOGY

The research methodology is illustrated through the provided flow chart in Figure 3.1.

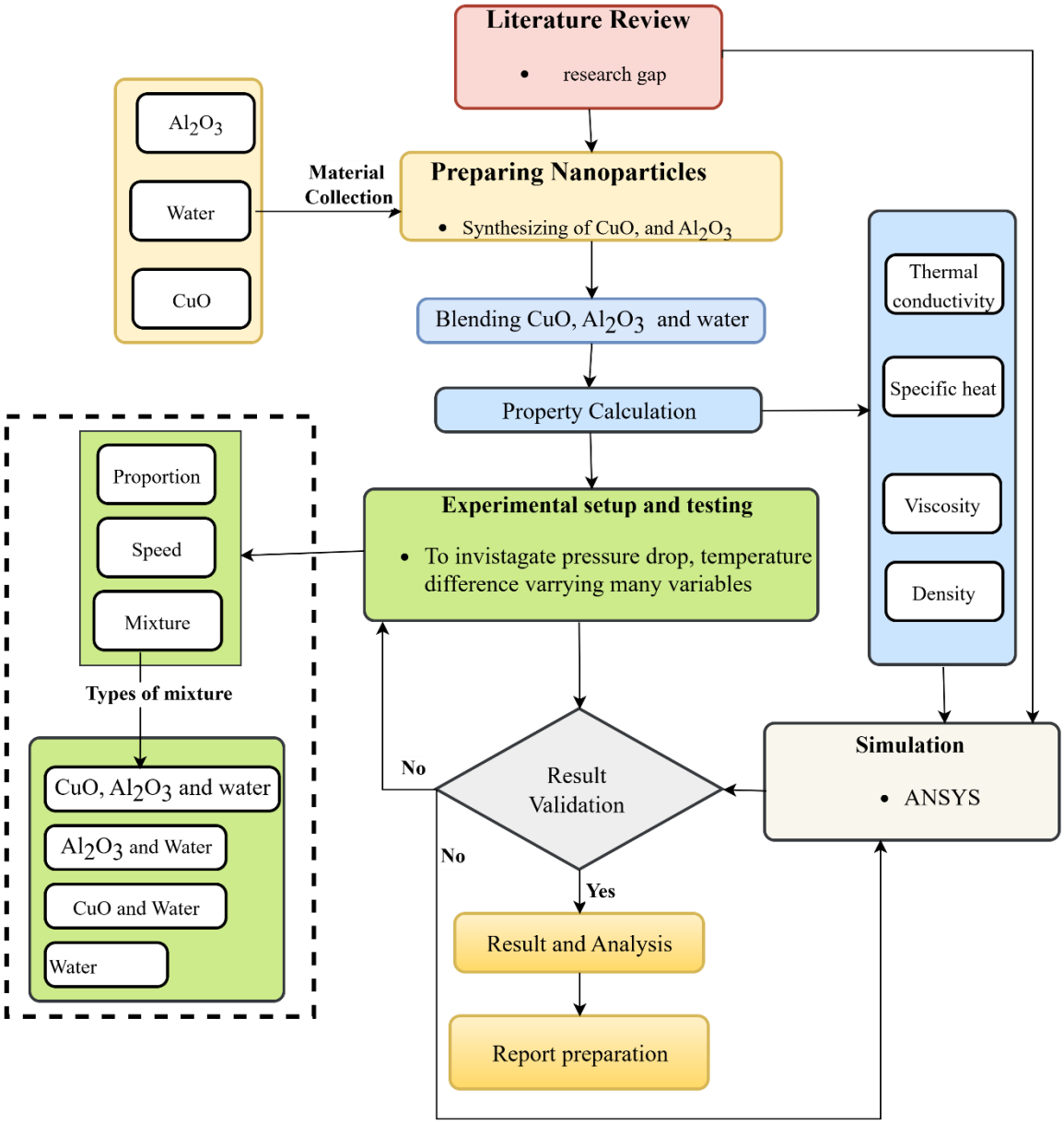

Figure 3. 1: Schematic diagram of research process

3.1 Literature Review

The selection of a possible research topic is the first step toward a successful research project, necessitating careful analysis and alignment with current scientific and technical developments. During literature study, previous studies, conclusions, and theoretical frameworks were thoroughly scrutinized to discover gaps and chances for original contributions.

From the previous study, it was found that there was minimum research has done in the hybrid nanoparticles. From intensive study, it was seen that there was limited research has conducted on the mixture of Al_2O_3, CuO and distilled water.

So, in this research Al_2O_3 and CuO nanoparticle was taken to synergistically enhance thermal conductivity and specific heat capacity.

I. Selection of Al_2O_3

- Al_2O_3 is the widely used nanoparticle to make nanofluid for the heat transfer analysis.
- It has high thermal conductivity, chemical stability, and is non-toxic.
- Comparing with other metal oxides, Aluminum Oxide is inexpensive and has a low density.
- It disperses properly in the distilled water.
- The nanoparticle with the size of less than 50 nm to increase the surface area was used in this study because of its excellent property.

II. Selection of CUO

- CuO is extensively studied as single nanoparticle.
- Though it is expensive than Al_2O_3, CuO was selected because of its high thermal conductivity than Al_2O_3.
- CuO along with Al_2O_3 was used to improve heat transfer by balancing density, viscosity of nanoparticle.
- The average size of the copper oxide taken was less than 50 nm a with 99% purity.

III. Selection of Distilled Water

- Distilled water was taken as a base fluid based on the previous extensive study, widespread application in heat exchanger.
- It is easily accessible, cost effective and has a stable physical property.
- It has low viscosity and relatively high specific heat capacity.
- It is safe to use with metal oxide.

IV. Selection of concentric heat exchanger

- Concentric heat exchanger was chosen because of its simplicity, ease of fabrication.
- There is high surface contact between two tubes which ensure increase of heat transfer rate.

3.2 Synthesis of Nanoparticles

Nanoparticles can be developed utilizing a variety of ways, including physical, chemical and procedures. Here are some popular methods in each category:

3.2.1 Synthesis of Al_2O_3 nanoparticles (Aluminum Oxide)

Al_2O_3 nanoparticles was synthesized using Sol Gel process in the chemistry lab in Department of Applied Sciences and Chemical Engineering, Pulchowk Campus. Procedure followed is mentioned below. (Owolabi & Ojadi, 2023) Carried out similar process.

- 10 gm of Aluminum Nitrate Nonahydrate ($Al(NO3)_3 .9H_2O$) was weighed in the analytical balance and dissolved in 100 ml of water with the help of magnetic stirrer in a beaker.
- Subsequently, ethanol (3.35 gm) was mixed with 50 ml of distilled water. And combined with Aluminum Nitrate Nonahydrate solution.
- The solution was placed in hot plate magnetic stirrer for one hours maintaining temperature of 80 degree Celsius, transparent solution was formed.
- Then gel was again heated in the muffle furnace at 350C for 45 minutes,
- Then the material obtained product was grounded and heated at 1000 degree Celsius for 1 hour resulting in the formation of Al_2O_3 nanoparticles.

3.2.2 Synthesis of CuO (Copper (II) Oxide) nanoparticles

Copper (II) Oxide nanoparticles was synthesized using the Sol-Gel Method in the chemistry lab in Department of Applied Sciences and Chemical Engineering, Pulchowk Campus. Procedure followed is mentioned below.(Radhakrishnan & Beena, 2014) followed the similar procedure.

- 2.5 gm of CuSo4.5H2o was taken in the weigh paper and measured in the analytical balance and dissolved with 100 ml of distilled water with the help of magnetic stirrer.
- A solution of sodium hydroxide was made by dissolving 4 grams of NaOH in about 100 milliliters of distilled water.
- About 5 ml of citric acid was dissolved in CuSo4 solution and taken in the flask and NaoH solution was added dropwise, black precipitate of copper Oxide was seen immediately.

- The precipitate obtained was filtered and washed several time to separate from the solution.
- To dry the obtained product, they were kept in Porcelain Basin and again heated in the muffle furnace at 500 degree Celsius for three hours.

3.3 Nanofluid Preparation

For this study, thermophysical properties used for CuO and Al_2O_3 Nanoparticle were used is shown in table Table 3.1 (Alosious et al., 2017).

Table 3. 1: Properties of Nanoparticles

Material	Al_2O_3	CuO
Diameter	<50nm	<50nm
Purity	99%	99%
Density	3970 kg/m3	6510 kg/m3
Specific Heat Capacity	525 J/kgK	540 J/kgK
Thermal Conductivity	17.65 W/mK	33 W/mK

For the preparation of nanofluid, two-step method was used. The fixed volume concentration of nanoparticle was taken I.e. $\varphi = 0.1$ % .But the proportion of the Al_2o_3: Cuo were varied to study the effect of proportion. Three different cases were established which are shown in following Table 3.2.

Table 3. 2: Proportion of *CuO: Al_2O_3* (Three different cases)

Proportion Of CuO: Al_2O_3	**CuO**	**Al_2O_3**	**Case**
25:75	0.025%	0.075%	C-1
50:50	0.050%	0.050%	C-2
75:25	0.075%	0.025%	C-3

Step 1: Measurement of nanoparticles:

The required amount of Copper (II) Oxide (CuO) and Aluminum Oxide (Al_2O_3) nanoparticles were precisely weighed using digital electronic balance which is shown in Figure 3-2. The amount depends on the desired concentration of the final nanofluid .

Figure 3. 2: Measurement of Cuo nanoparticle

Step 2: Dispersion of CuO and Al_2O_3 in Base Fluid.

At first Cuo was added to the beaker containing base fluid and it was stirred with magnetic stirrer for 5 minutes. After that, Al_2O_3 was added on the mixture of cuo and base fluid, while continuously agitating. This hybrid nanofluid was mixed for more five minutes in the stirrer.

Step 3: Sonication of hybrid nanofluid

After mixing cuo and Al_2O_3 in base fluid, the beaker was transferred to the ultrasonic cleaner with ultrasonic frequency of 40 KHZ. To blend the mixture properly the sonication process was done for 90 minutes. After the process, there was no any agglomerations of particle. To prevent agglomerations of particle, the experiment was conducted within 5/6 hour from the sonication process. Figure 3.3 shows the Cuo-Al_2O_3-water hybrid nanofluid after sonication process.

Figure 3. 3: Cuo-Al_2O_3-water after sonication

3.4 Properties of nanofluid

Testing the characteristics of nanofluids is critical for understanding their behavior and possible uses, particularly in heat transfer and cooling systems. Thermal conductivity, viscosity, specific heat capacity and density were calculated theoretically.

3.4.1 Viscosity

The viscosity was calculated using the following formula (Vajjha et al., 2010)

Batchelor model: $\mu hnf = \mu f\ (1 + 2.5 * Ø + 6.2 * Ø^2)$ Equation 3. 1

Where, μhnf is viscosity of hybrid nanofluid

μf is viscosity of base fluid

Ø is volume concentrations of hybrid nanoparticles

3.4.2 Density

The density of Al2O3and CuO nanoparticles are considered as temperature-independent throughout the operational range. Water, on the other hand, has a temperature-dependent density. Changing water density while maintaining a steady flow rate affects heat transmission between the cold and hot sides of a heat exchanger.

The hybrid nanofluid's density was calculated in relation to the mass fraction of nanoparticles.(Ho et al., 2010)

$$\rho hnf = Ø1(\rho)CuO + Ø2(\rho)Al^2O^3 + (1 - Ø)(\rho)f \quad \text{Equation 3. 2}$$

Where, ρhnf is density of hybrid nanofluid

Ø1 is volume concentrations of CuO nanoparticles

Ø2 is volume concentrations of Al_2O_3 nanoparticles

(ρ)CuO is density of CuO nanoparticles

(ρ)Al_2O_3 is density of Al_2O_3 nanoparticles

(ρ)f is density of base fluid

Ø (Ø1+ Ø2) is volume concentrations of hybrid nanoparticles

3.4.3 Specific heat capacity

The specific heat of hybrid nanofluids was calculated with following expression (Ho et al., 2010; Shaik et al., 2024)

$$(\rho Cp)hnf = Ø1(\rho Cp)CuO + Ø2(\rho Cp)Al_2O_3 + (1 - Ø)(\rho Cp)f \quad \text{Equation 3. 3}$$

Where, Cphnf is Specific Heat Capacity of hybrid nanofluid

(Cp)CuO is Specific Heat Capacity of CuO nanoparticles

(Cp)Al_2O_3 is Specific Heat Capacity of Al_2O_3 nanoparticles

(Cp)f is Specific Heat Capacity of base fluid

3.4.4 Thermal conductivity

In the literature review, it was discovered that multiple models are employed to estimate the thermal conductivity of nanofluids. These models take into account several elements, such as thermal conductivity of the nanoparticles, fluid , along with shape, size, temperature. In this research, the thermal conductivity of hybrid nanoparticle was determined via following equation (Hassaan, 2024)

$$\frac{khnf}{kf} = \frac{\frac{(Ø1k1 + Ø2k2)}{Ø} + 2kf + 2\,(Ø1k1 + Ø\,2k2) - 2Ø\,kf}{\frac{Φ1k1 + Ø\,2k2}{Ø} + 2kf + 2\,(Ø1k1 + Ø\,2k2) + Ø\,kf} \quad \text{Equation 3. 4}$$

Where, Khnf is Thermal Conductivity of hybrid nanofluid

K1 is Thermal Conductivity of CuO nanoparticles

K2 is Thermal Conductivity of Al_2O_3 nanoparticles

Kf is Thermal Conductivity of base fluid

3.5 Experimental setup

The experimental setup for a concentric heat exchanger was developed to investigate its performance under different operating conditions. In a counter-flow system, heat and cold fluids move in opposite directions. Counter-flow heat exchangers was selected because they are more efficient than parallel-flow heat exchangers. They maintain a greater temperature difference between fluids throughout their length, resulting in a higher LMTD and more heat transfer (Krasniqi et al.,2018) .

The pressure drops and temperature difference across the heat exchanger at different flow rates are measured using various nanofluid proportions and combinations. The setup consists of primary and secondary heat exchanger, three pumps, two pressure sensor, four thermocouples, two flow sensors, hot water collector etc. The detailed view Figure 3.4.

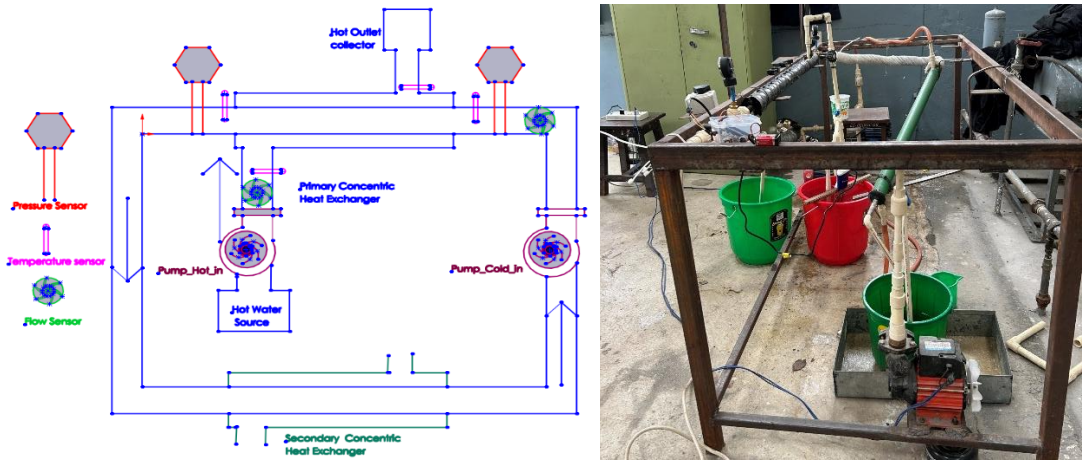

Figure 3. 4: Experimental setup

The setup consists of mainly following components:

3.5.1 Primary Concentric heat exchanger

This is the main part of the experimental system, temperature, pressure, flow rates etc. are measured across this section. The material of tube is copper, whereas the material of shell is CPVC . The shell has external diameters of 35 mm and internal diameters of 27mm and has a thickness of 4 mm. The shell is covered with the insulator to prevent heat loss to the surrounding. The tube has external and interior diameters of 13 mm and 10 mm, respectively, with a 1.5 mm wall thickness. The length of the shell and tube is 1000 mm and 1060 mm respectively. The detailed dimensions are mentioned in the following Figure 3.5 and Figure 3.6.

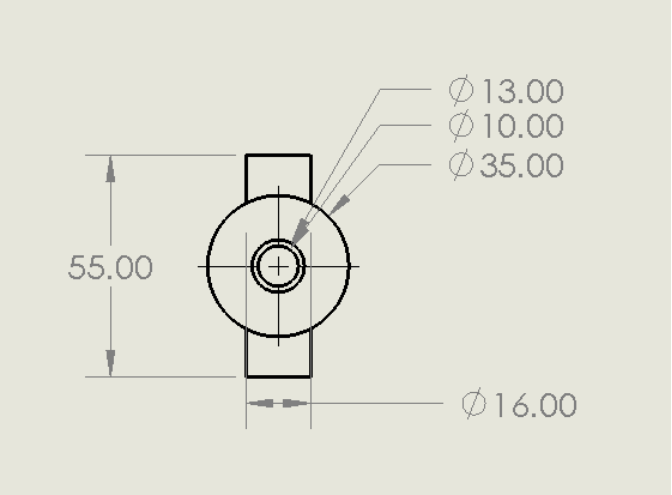

Figure 3. 5: Size of the tube and shell

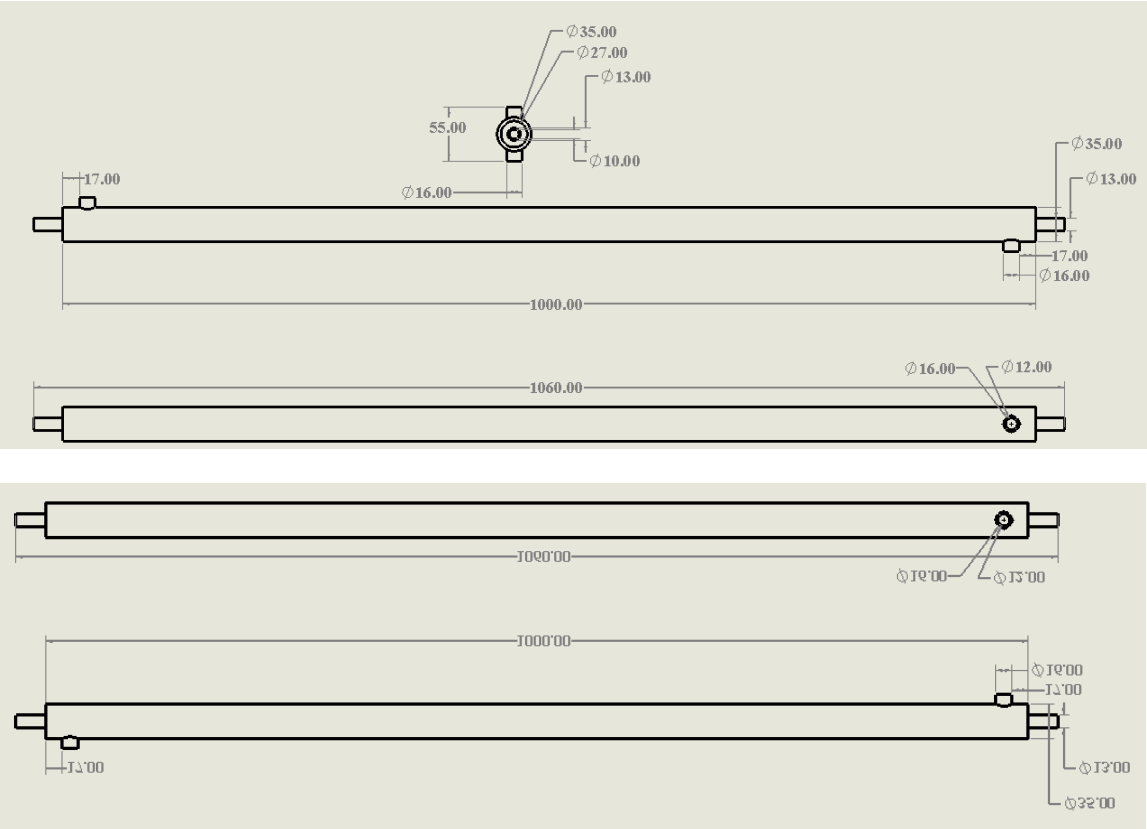

Figure 3. 6: Detailed dimension of concentric heat exchanger

3.5.1.1 Thermocouples

Two openings with a diameter of 2mm are made at both the entrance and exit of the copper tube, and two thermocouples are placed to record the temperatures of the cold nanofluids at the inlet and outlet. In the same manner, two additional holes with a diameter of 2mm are made at the inlet and outlet of the CPVC shell, and two thermocouples are positioned to record the inlet and outlet temperatures of the hot water. All four

thermocouples underwent calibration in a thermostat with a ± 0.1°C fluctuation prior to usage. Temperature measurements were taken with digital thermocouples, and average figures were utilized for analysis. The hot fluid transfers heat, raising the temperature of the cold nanofluid and lowering the temperature of the hot fluid.

3.5.1.2 Pressure Sensor

At the entrance and exit of the copper tube, two pressure gauges are placed to assess the initial pressure of the nanofluid and the pressure drop following heat transfer in the heat exchanger.

3.5.1.3 Flow Sensor

Two flow sensors are placed at the entry section of the copper tube and outer shell to gauge flow rate of hot water and cold nanofluids. Flow readings were recorded using a computer and Arduino, and average values were used for analysis.

3.5.2 Secondary Concentric heat exchanger

The main function of secondary heat exchanger is to maintain the inlet temperature of the cold nanofluid since nanofluid was re-circulated across the system. The tube is constructed from aluminium, while the shell is composed of CPVC. The shell has external diameters of 40 mm and and internal diameters of 32 mm and has a thickness of 4 mm. The tube has external and interior diameters of 15 mm and 13 mm, respectively, with a 1 mm wall thickness. The length of the shell and tube is 1000 mm and 1180 mm respectively.

3.5.3 Pump

Three pumps are installed in the system to circulate. Pump 1 and pump 2 are used to circulate the hot water and cold nanofluid in the primary heat exchanger, whereas pump 3 is used to circulate coolant (Cold water) in secondary heat exchanger to maintain the steady inlet temperature of the cold nanofluids.

3.5.4 Collector

Two buckets are used to store the hot water as hot water was not re-circulated throughout the system and only one bucket is used to collect cold nanofluid as it was re-circulated throughout the system.

3.6 Material collection, Fabrication and Assembly

After collecting different components and materials, fabrication as well as assembly of the component to make the experimental setup involved following steps.

a. Fabrication of two heat exchanger

After creating the experimental setup layout, the dimensions are finalized for two heat exchanger. Primary heat exchanger is made with copper tube and CPVC shell. Secondary heat exchanger is made with aluminum tube and CPVC shell.

b. Fabrication of frame

After creating heat exchanger, the dimension required for the frame is finalized. The square shapes cast iron was purchased, measured and cut in required dimension. After that, the frame is created by welding procedure to support different component of the system.

c. Fabrication of helical coil turbulator

Two different size of helical coil turbulator are fabricated using mild steel wire of diameter 1 mm. The diameter of coil is 9 mm and pitch is 12mm and 18 mm. Turbulators are used to experiment pressure drop across the system.

d. Re-circulation system for fluid

After the fabrication of the frame, the closed CPVC pipe system is fabricated to circulate the cold fluid. In addition, CPVC pipe is fitted for the hot fluid.

e. Installation of pump and water supply

Two different pumps are used to supply hot and cold fluid in the system. The third pump was installed to circulate coolant from the underground tank.

f. Installation of water Heater

To heat the water, immersion water heater rod with 1500 W capacity was installed in the system.

g. Installation of Different Sensors

A pressure gauge connects to both the Outlet and Inlet sides of the tube to monitor pressure. Two flow meter are attached at inlet section of tube and shell to monitor the inlet flow rate . Four thermocouples were placed at the outlet and inlet sides of the tube

and shell to measure temperature. After assembling all the components, the system was run for 5 minutes to check the leakage in the system.

3.7 Experimental Procedure

After the fabrication of experimental setup, experimental procedure began. The process involved the following steps.

- Step 1: The water tank for secondary heat exchanger is filled, all the pumps, sensor etc. are checked. The Hot water is pre-heated at the temperature of 70° C. The nanofluid is collected in the collector.
- Step 2: All the components are checked, different pump are run separately to check to leakage.
- Step 3: The flow sensors are connected to the Arduino, the temperature sensors and pressure gauge are observed.
- Step 4: All three pumps are run simultaneously and ball valve are adjusted according to the desire flow rate.
- Step 5: After the system reached in steady state conditions. The major data such as inlet outlet temperature for cold and hot fluid are recorded. In addition to pressure and flow rate are also measured for the steady state condition.
- Step 6: The same procedure was repeated by varying the operating conditions, varying the concentration of hybrid nanoparticle in the base fluid.

3.8 **Methods available for Heat Transfer analysis**

There are three methods available for analysis of heat transfer analysis.

3.8.1 Analytical /Theoretical method

Analytical method only works for simple cases and laborious. They are only possible for limited number of problems. Employ principles and related formulas like Newton's laws of viscosity to address fluid flow issues.

3.8.2 Experimental method

Experimental method is accurate but limited and expensive, also sometimes time consuming. We need to create specialized facilities, incur high construction expenses, and ensure they are precisely calibrated and meticulously designed. They conduct experiments to grasp the phenomena and relationships among different variables, like

wind tunnel tests that aid in designing and optimizing the external shapes of aircraft, vessels, vehicles, etc.

3.8.3 Numerical method

This method is as accurate as experimental method and cheaper. This also provides lot of flexibility of analytical methods. ANSYS software can be used to solve variety of issue related fluid dynamics.

3.9 CFD (Computational fluid dynamics)

Computational fluid dynamics (CFD) is a computer software that is used to simulate the fluid dynamics in numerical context. They use equations such as Navier-Stokes (momentum conserved), continuity (mass conserved) and energy equation (energy conserved) to solve flow problems. It is computational transport phenomenon which involve heat, mass transfer or any other transport phenomenon within it.

There are various tools used in analysis of Heat Transfer analysis. Here, ANSYS software is used to evaluate the heat exchanger's performance under various scenarios. Ansys software is a powerful, versatile fluid dynamics application designed to address fluid flow challenges employing various turbulence models. The program was selected because of the existing literature and personal familiarity with the software. This includes comparing pressure drop and temperature changes at different flow rates and nanofluid combinations. Using ANSYS, deep insights into the heat transfer characteristics and optimize the design for greater efficiency. The general steps involved are shown in Figure 3.7.

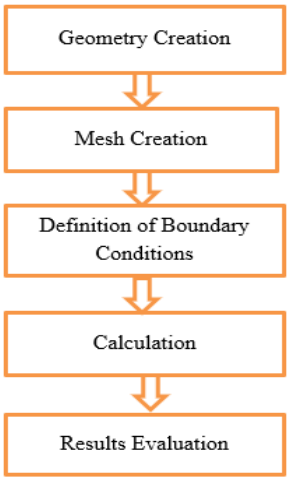

Figure 3. 7: CFD process for simulation

3.10 Grid Independent Test (GID) Test

A well- defined grid is crucial for generating satisfactory outcomes in fluid dynamics simulations, and the selection of properties influences the accuracy and convergence of the solution. In this study, at first grid independence test was carried out for water as hot fluid and cold fluid; using the following geometry, meshing, and boundary conditions. After this test, the result were analysed and one coarser mesh with the finest result is taken for further analysis keeping all the common parameter, geometry and methods constant. All other analysis were conducted by varying the fluid properties and boundary conditions.

The produced solution is reliable solely if it is unaffected by the mesh. To meet these criteria, a mesh independence test is required. An example of this kind of test is listed in (Leap CFD Team, 2012). For the mesh to be independent three criteria must be met:

- Residual RMS Error figures have decreased to a satisfactory level (usually 10-4 or 10-5).
- Keep track of points until the values of interest stabilize.
- The domain exhibits imbalances of under 1% of the variables.

If these conditions are satisfied and the outcomes are consistent across various meshes, then they are mesh-independent. Once the mesh independency is established, the least dense independent mesh is selected to reduce simulation time, as the outcomes should remain consistent.

The GID test was performed to choose the final model for further simulation. The test was done in steady state. Two different points are taken for GID test.

Point 1: Cold Outlet (-30, 0, 0)

Point 2: Hot Outlet (975, -25, 0)

3.10.1 Geometry Creation

To conduct a CFD analysis, a 3D model of the heat exchanger is first created using the necessary design specifications. In this study, the CFD analysis is conducted using ANSYS Workbench.Ansys design modeler is used to create the geometry of concentric heat exchanger which in Figure 3.8.

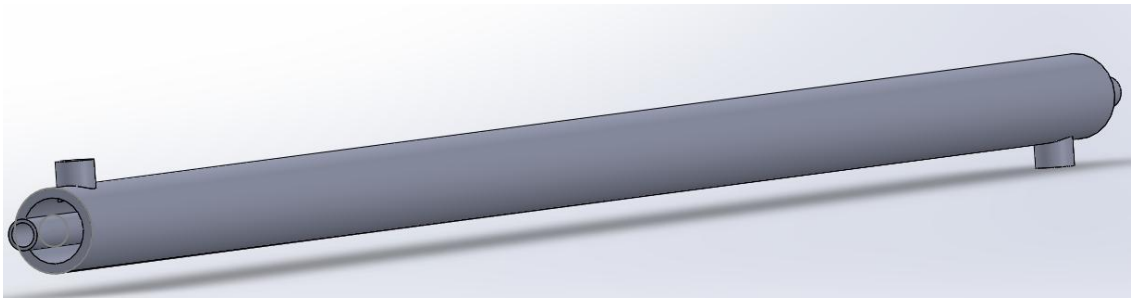

Figure 3. 8: Geometry Created in Ansys Design Modeler

3.10.2 Mesh creation

Mesh simply means dividing given physical domain into small sub domains (cells or elements). It is needed because:

- It refers to the cells or elements where the flow is resolved.
- It is a discrete representation of geometry of problem.

Generally, there are two types of mesh:

i Structured Mesh

- Recognized through consistent connectivity.
- Element selections are quadrilateral in two dimensions and hexahedral in three dimensions.
- Extremely space-efficient.
- Benefits include improved convergence and enhanced resolution.

ii Unstructured Mesh

- Identified by irregular connectivity.
- Can be highly space inefficient compared to structured mesh.
- Employ triangle in 2D and tetrahedral in 3D.

After creating the geometry, the geometry is exported for meshing. Meshing is done using the default mesh setup and only varying the mesh size. Geometry have both structured and unstructured mesh. The meshing structures available for different types of size are shown below.

(a) 5403245-coarser

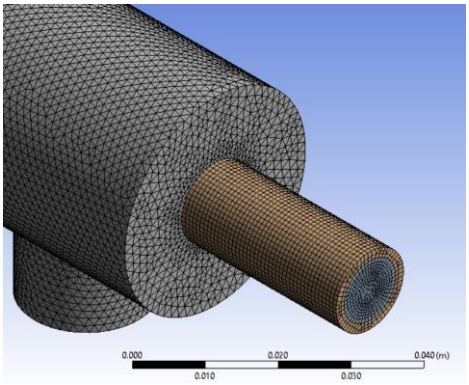

(b) 6772388-coarse

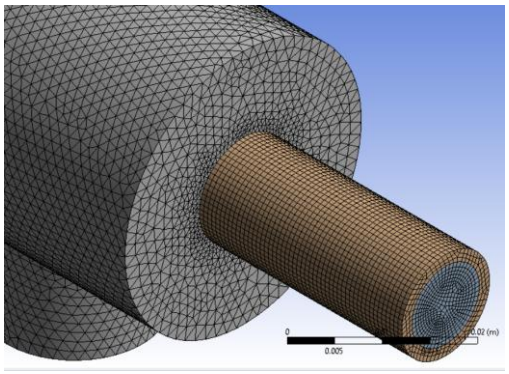

(c) 8608563 (fine)

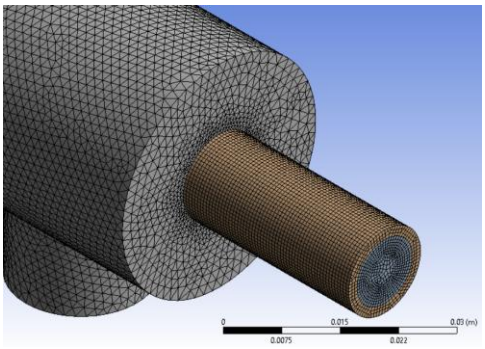

(d) 8839933 (Finer)

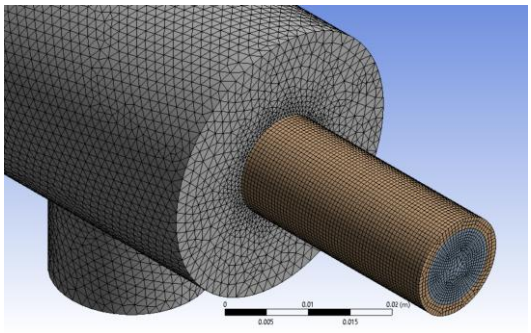

Figure 3. 9: Mesh structure with number of elements

Four different types of mesh created for the grid independent test are shown in Figure 3.9 a, b, c and d shown the coarse and coarser mesh structure and the fine mesh having elements no of 8839933 is shown in figure (d).

3.10.3 Boundary Conditions and Setup requirements

Boundary conditions are most important parameter to accurately replicate any issue domain. Properly defining these parameters is crucial for accurate and reliable findings. Boundary conditions are frequently derived from practical uses, whereas others are established through techniques in simulation software. This section defines the boundary conditions for the geometric model's components. The ANSYS solver uses numerous constraints linked to the problem domain to generate equations. Simulation software interprets physical or practical boundary conditions. The concentric heat exchanger's boundary condition for both the tube and shell outlets is set to a pressure outlet. The boundary conditions as well as setup requirements is shown in Table 3.7.

Table 3.3: Setup requirements

Time dependent	Steady
Turbulence	K-epsilon, Realizable
Energy	ON
Gravity	ON
Boundary Conditions	Cold Velocity Inlet: 1.27 m/s
	Temperature:30^0 C
	Outlet: Pressure outlet= 0 Pa
	Hot Velocity Inlet: 0.38 m/s
	Temperature:70^0 C
	Outlet: Pressure outlet= 0 Pa
Methods	Coupled
Residual	10e-^{6}
Initialization	Hybrid

The density, specific heat capacity, and thermal conductivity of copper tube are 8978 kg/m³, 381 J/kg K, and 387.6 W/m K, respectively.

3.10.4 Solution Method and Initialization

In ANSYS Fluent, the solution of governing equations can be discretized using two methods: the first-order upwind technique and second-order technique. For first-order technique, the value at the face of the cell matches that of its central cell. The second order approach, on the other hand, solves the governing equations using Taylor series expansion. Since, first order technique is less computationally expensive, ANSYS Fluent suggests adopting it for cases where the maximum level of precision is not essential. On the other hand, despite the longer computing time, the second order approach is advised when the maximum accuracy is needed in the solution. In this case, second order upwind solution method and hybrid initialization was used.

CHAPTER FOUR: RESULTS AND DISCUSSION

4.1 **Characterization of Nanoparticles**

Al_2O_3 and CuO nanoparticles were produced using the sol-gel process and assessed for physical and structural properties prior to blending to base fluid. The phase and crystalline structure were investigated using X-ray diffraction (XRD), which revealed the presence of sharp peaks corresponding to both nanoparticles demonstrate a high degree of crystallinity.

The crystallinity, phase purity, and particle size of the produced nanoparticles were measured by X-ray diffraction. The incident X-ray is diffracted by the nanoparticles in accordance with Bragg's law, resulting in peak intensities and associated peak positions.

4.1.1 XRD Analysis of CuO

The Miller Indices obtained from XRD data of CuO are -111,111, -202,202,-113,022 and 220 is shown in Figure 4.1 are in good concordance with the data obtained by (Sagadevan et al., 2017) ;Radhakrishnan and Beena, 2014) No other peaks were seen, which indicates the formation of pure CuO nanoparticle. The average size of the nanoparticle produced was 33 nm which was calculated using scherrer equation.

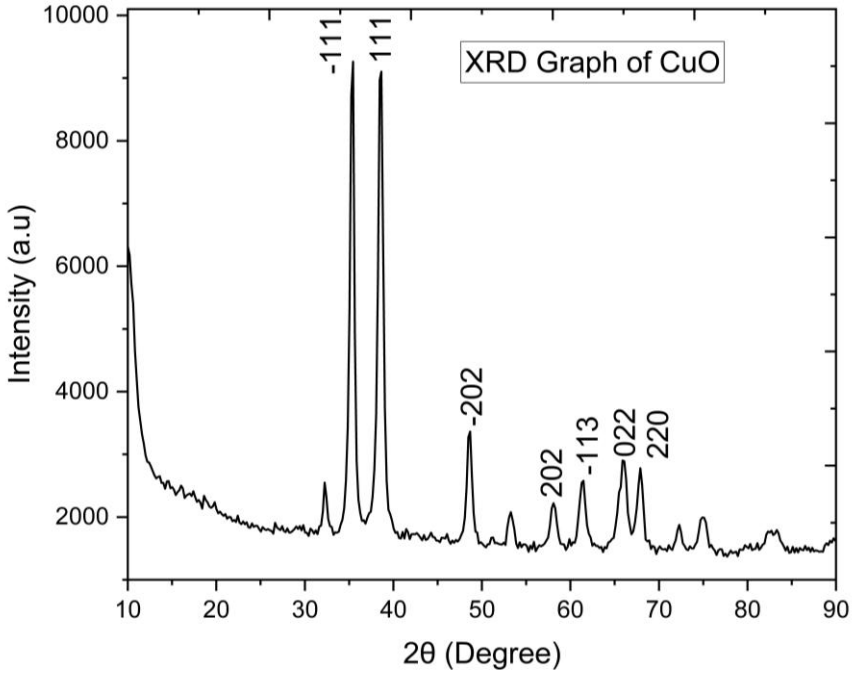

Figure 4. 1: XRD Graph of CuO

4.1.2 XRD Analysis of Al_2O_3

The Miller Indices obtained from XRD data of Al_2O_3 Nanoparticle are 012, 104, 110, 113 ,202, 024, 116 and 214 is shown in Figure 4.2 are in good concordance with data obtained by (Owolabi and Ojadi, 2023).No other peaks were seen, which indicates the formation of pure Al_2O_3 nanoparticle. The average size of the nanoparticle produced was 37 nm which was calculated using scherrer equation.

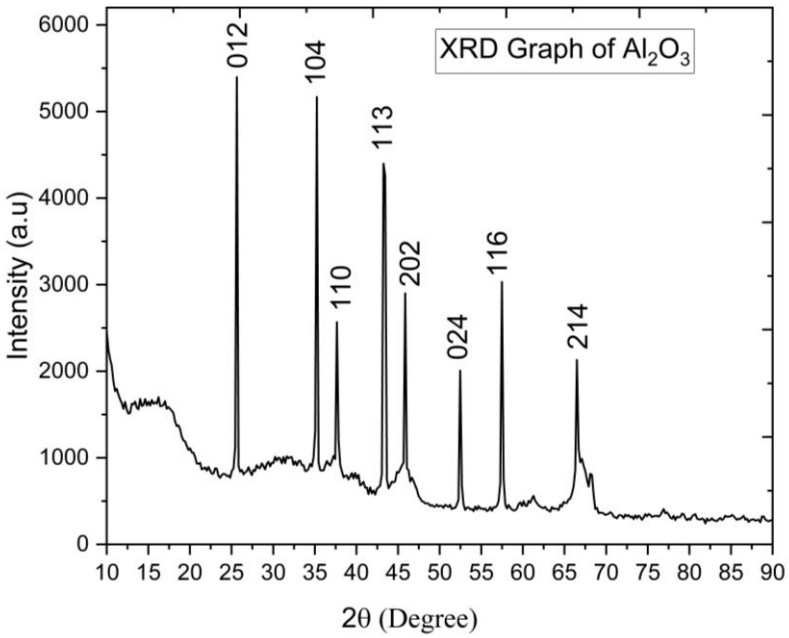

Figure 4. 2: XRD Graph of Al_2O_3

4.2 Simulation result

After all the required parameter for the simulation, setup was done at inlet, outlet, wall and boundary condition. Counter flow heat exchanger is used. CFD simulation solution result was taken after solution is converged.

4.2.1 GID Test

For GID test steady simulation was done for different mesh number. From Figure 4.3 and 4.4, it is seen that the temperature at cold outlet and hot outlet is almost steady while varying the no of elements. So, coarse elements (No of elements: 6772388) are taken for further simulation.

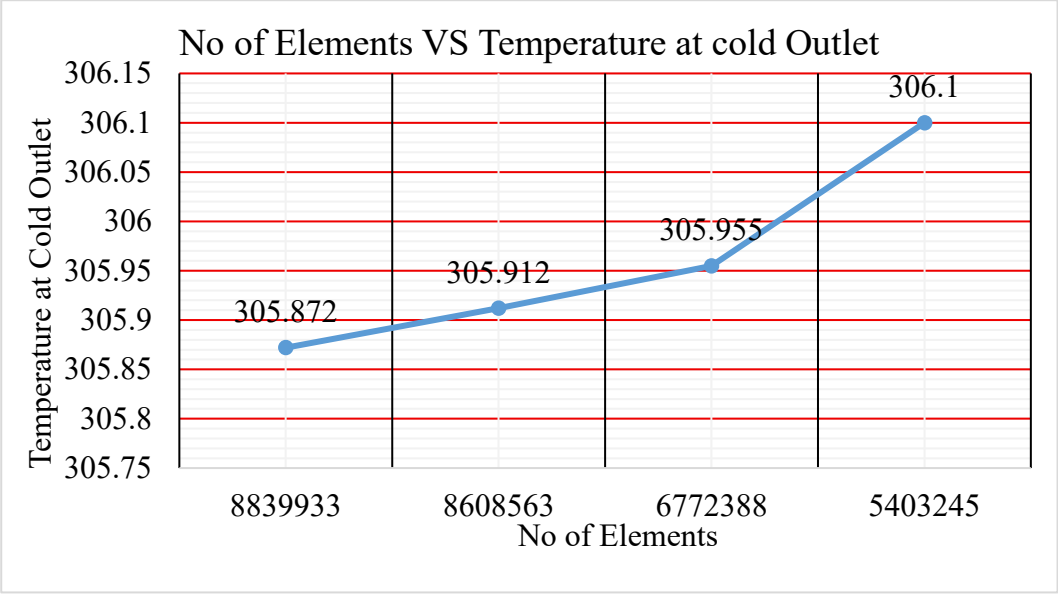

Figure 4. 3:No of Elements Vs Temperature at Cold Outlet

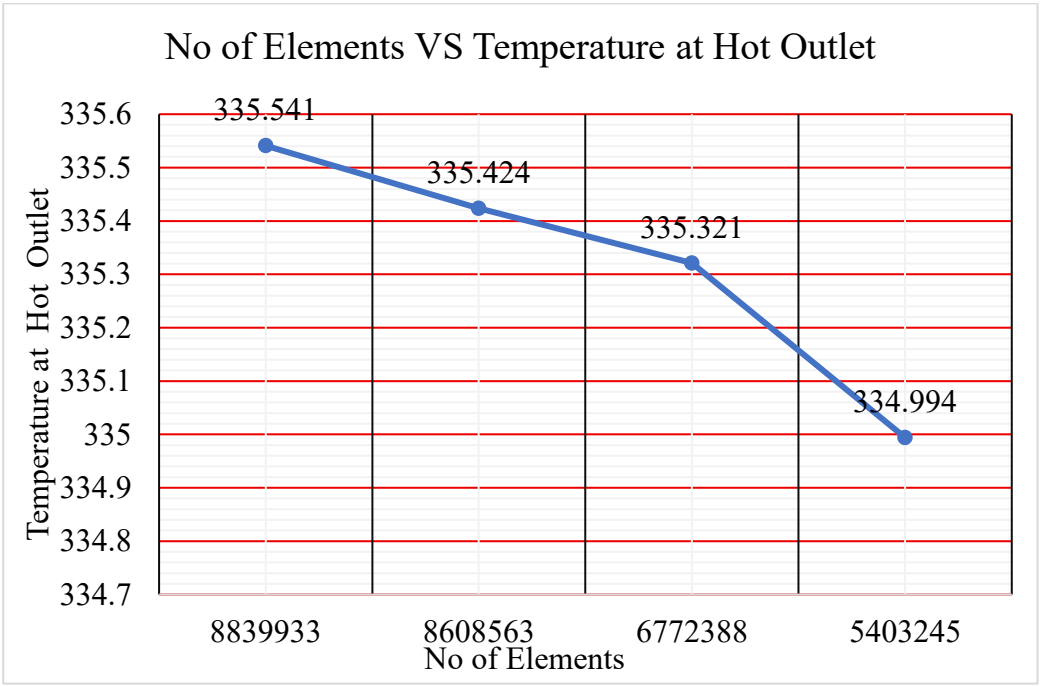

Figure 4. 4: No of Elements Vs Temperature at Hot Outlet

4.2.2 Simulation Result for distilled water

After completing the GID test, simulation was run for distilled water as cold fluid only. The flow rate for the cold fluid was varied keeping the flow rate of hot fluid constant. The results obtained for three different flow rates are shown below.

I. Cold fluid rate of 8.14 Liter Per Minute (LPM)

The flow rate for cold fluid is 8.14 LPM and flow rate for hot fluid is 5.99 LPM. The results obtained are shown below. Temperature Contour and Pressure Contour is shown in Figure 4.5 and Figure 4.6 respectively.

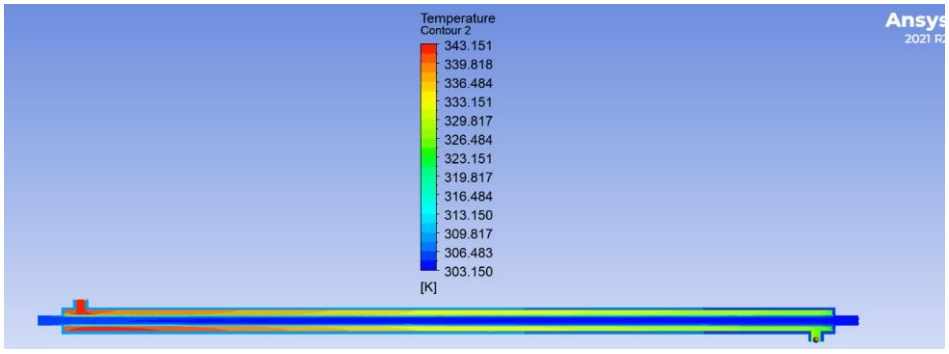

Figure 4. 5: Temperature contour

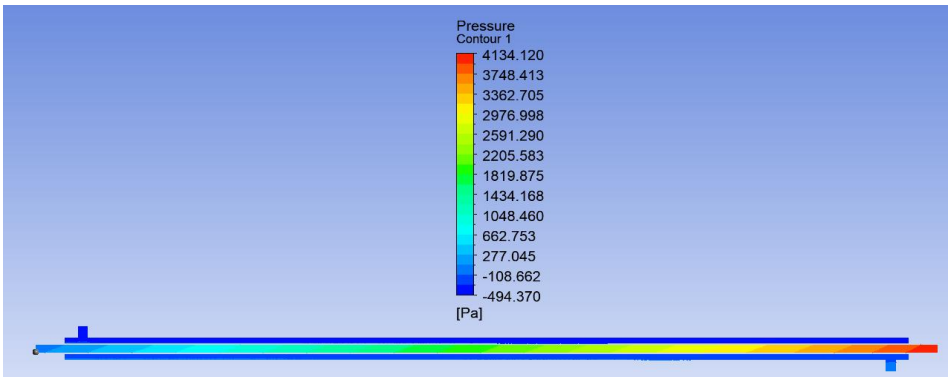

Figure 4. 6: Pressure contour

II. Cold fluid rate of 6.47 Litre Per Minute (LPM)

The flow rate for cold fluid is 6.47 LPM and flow rate for hot fluid is 5.99 LPM. The results obtained are shown below. Temperature Contour and Pressure Contour is shown in Figure 4.7 and Figure 4.8 respectively.

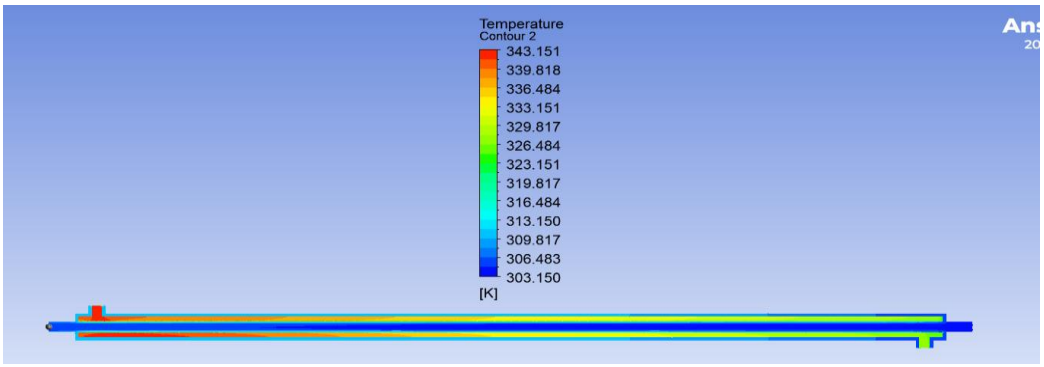

Figure 4. 7: Temperature contour

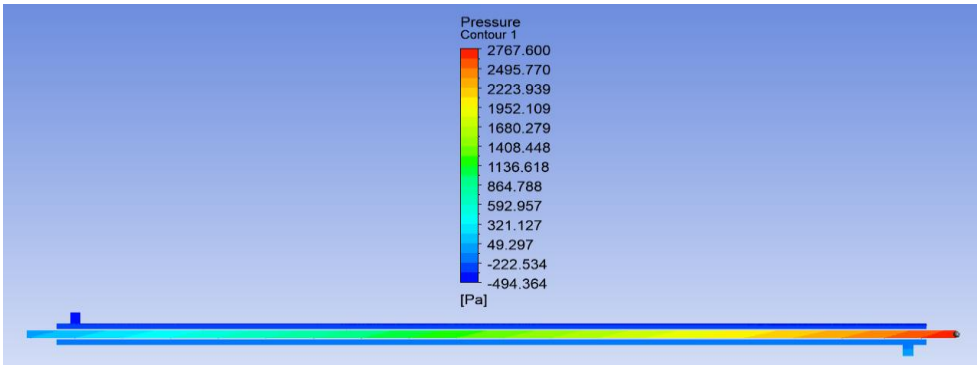

Figure 4. 8: Pressure contour

III. Cold fluid rate of 5.07 Litre Per Minute (LPM)

The flow rate for cold fluid is 5.07 LPM and flow rate for hot fluid is 5.99 LPM. The results obtained are shown below. Temperature Contour and Pressure Contour is shown in Figure 4.9 and Figure 4.10 respectively.

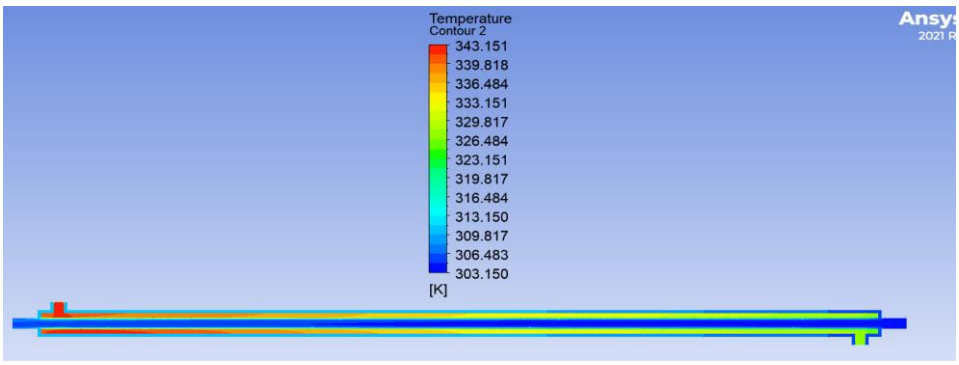

Figure 4. 9: Temperature contour

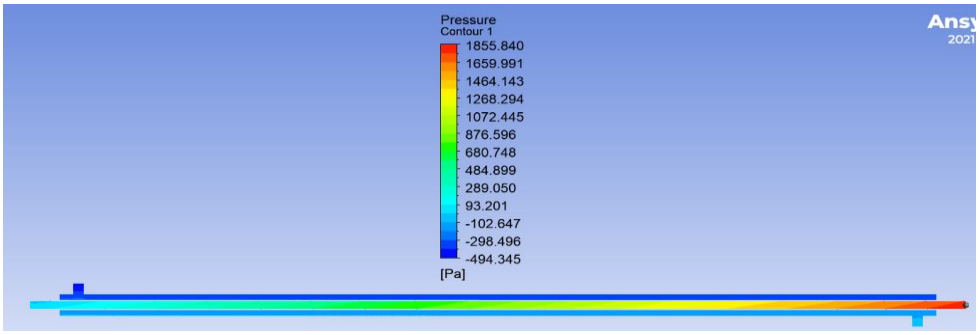

Figure 4. 10: Pressure contour

From above temperature contour it is seen that, the temperature of cold fluid is increasing and temperature of hot fluid is decreasing.

From above pressure contour it is seen that, the pressure of cold fluid is significantly dropped from inlet to outlet.

4.3 Comparison of Overall heat transfer coefficient (U) with varying flow rates (q) for water and various hybrid nanofluid proportion

When CuO nanoparticles and CuO-Al_2O_3 hybrid nanoparticles were introduced to distilled water, the overall heat transfer coefficients increased. Overall heat transfer coefficients for CuO (0.025 %) nanofluid; CuO-Al_2O_3(25:75); CuO-Al_2O_3(50:50); CuO-Al_2O_3(75:25) hybrid nanofluids increased by 5% to 8.64%;11.91 % to 18.7 %;16.21 % to 28.78 %; 20.67 % to 36.39 % respectively across flow rates ranging from 5.60 LPM to 10.4 LPM compare to distilled water. This improvement in the overall heat transfer coefficient results from the increased thermal conductivity offered by the nanoparticles added (Fares et al., 2020) .

Figure 4.11 shows the U versus different q for water and various hybrid nanofluid proportion and error bar shows the standard deviation.

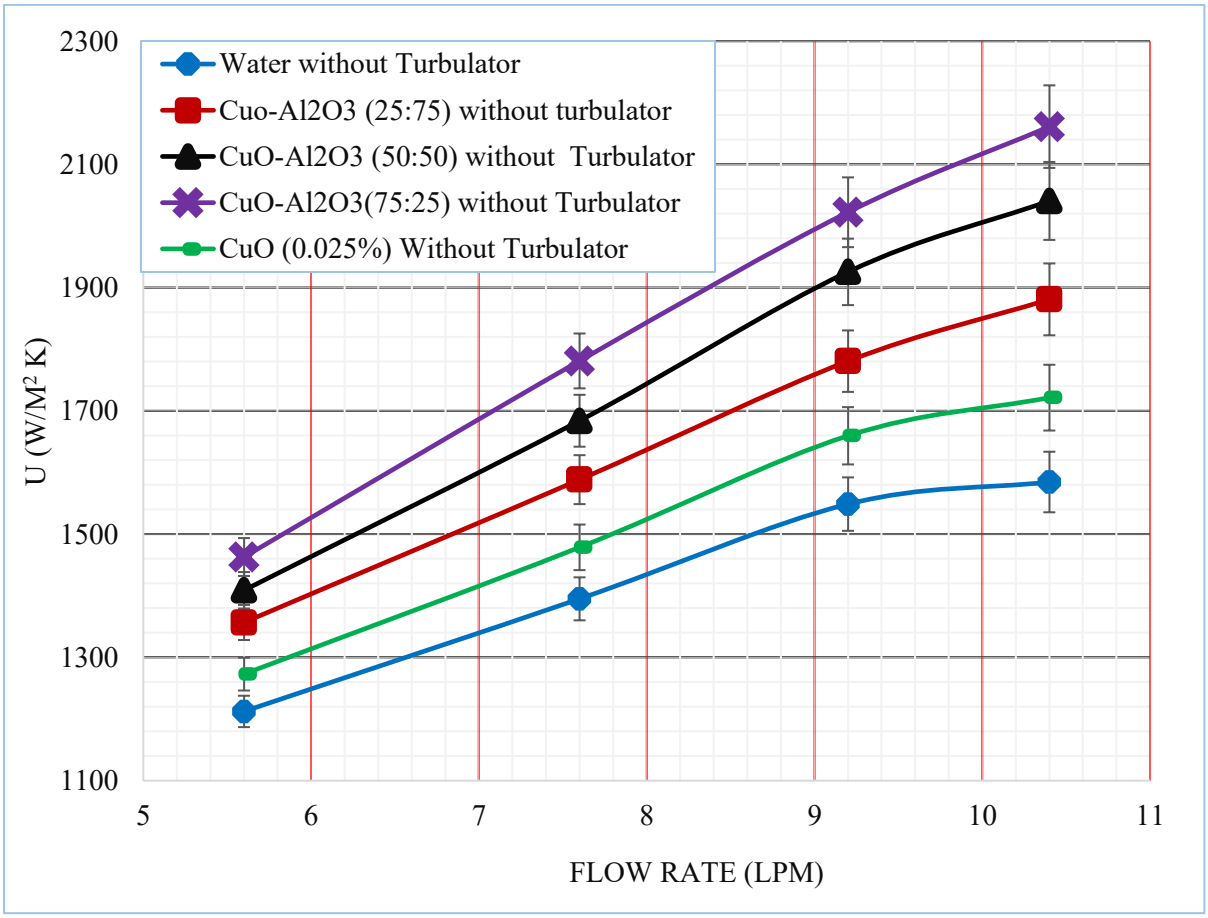

Figure 4. 11: U versus varying q for water and various proportions of hybrid nanofluid

4.4 Comparison of Overall heat transfer coefficient (U) with 18 mm turbulators for various hybrid nanofluid proportion

Overall heat transfer coefficients for CuO (0.025 %) nanofluid; CuO-Al_2O_3(25:75);CuO-Al_2O_3(50:50);CuO-Al_2O_3(75:25) hybrid nanofluids increased by 5.65% to 10.31% ; 13.88 % to 23.43 %;22.42 % to 35.46 %; 31.09% to 48.56 % across flow rates ranging from 5.60 LPM to 10.4 LPM with 18 mm pitch turbulator compare to distilled water.

Figure 4.12 shows the U versus different q with 18 mm turbulator and error bar shows the standard deviation.

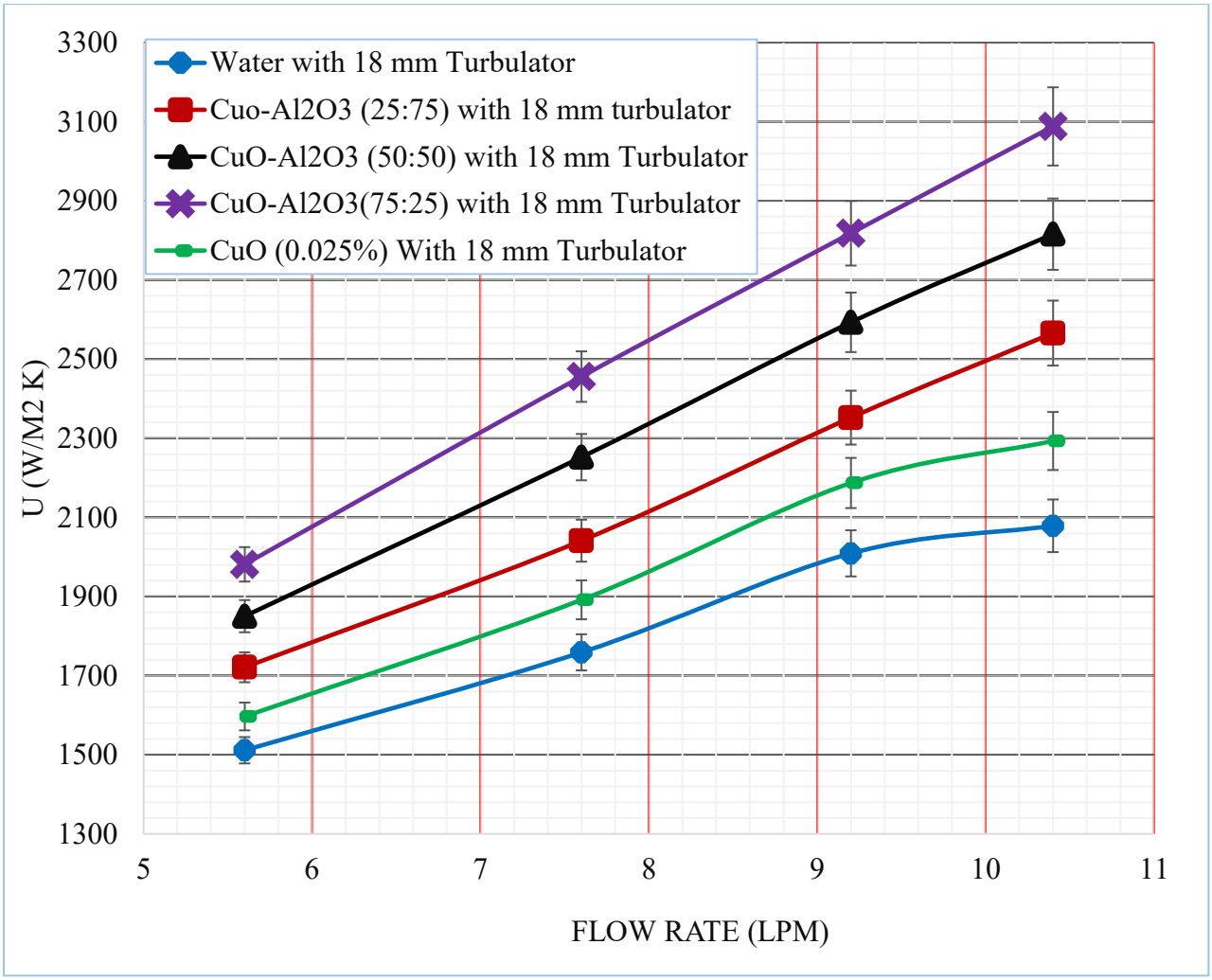

Figure 4. 12: U vs different q with 18 mm turbulator

4.5 Comparison of Overall heat transfer coefficient (U) with 12 mm turbulators for different hybrid nanofluid proportion

Overall heat transfer coefficients for CuO (0.025 %) nanofluid; CuO-Al2O3(25:75); CuO-Al2O3(50:50); CuO-Al2O3(75:25) hybrid nanofluids increased by 6.15 % to 11.54 % ;13.91 % to 23.76 %; 22.92 % to 36.28 %; 32.12 % to 49.44 % respectively across flow rates ranging from 5.60 LPM to 10.4 LPM with 12 mm pitch turbulator compare to distilled water.

Figure 4.13 shows the U versus different q with 12 mm turbulator and error bar shows the standard deviation.

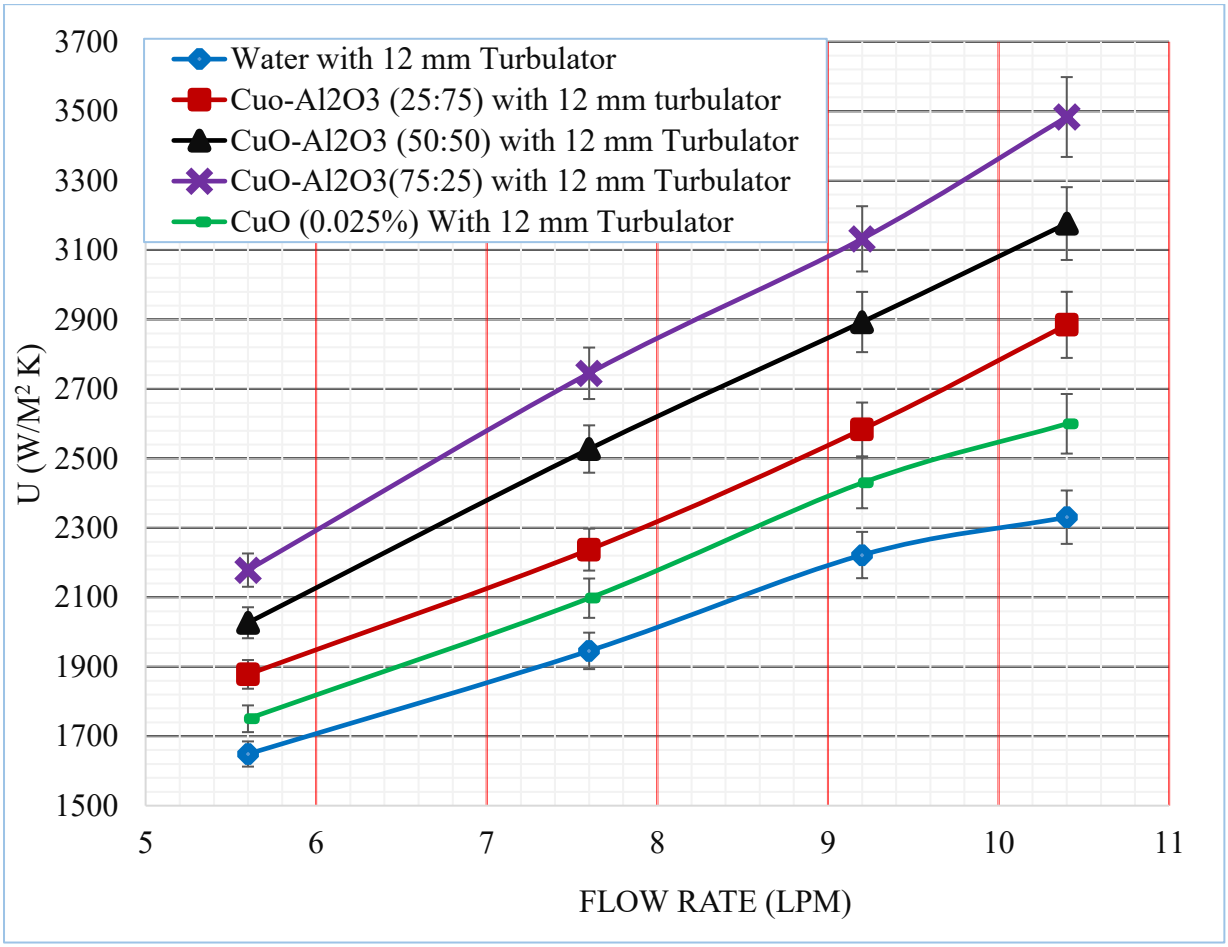

Figure 4. 13: U vs different q with 12 mm turbulator

4.6 Comparison of Overall heat transfer coefficient (U) with various turbulators for distilled water

Adding 18 mm pitch helical coil turbulator in the inner tube where cold fluid was flowing, overall heat transfer coefficients increased by 24.66 % to 31.18%; across flow rates ranging from 5.60 LPM to 10.4 LPM compare to distilled water without turbulator. Replacing 18 mm pitch with smaller pitch turbulator which is 12 mm, overall heat transfer coefficients increased by 36 % to 47.08 % across flow rates ranging from 5.60 LPM to 10.4 LPM compare to distilled water without turbulator. Helical coil turbulator with reduced pitch size increases turbulence, thereby improving heat transfer, in agreement with earlier studies (Akyürek et al., 2018) .

Figure 4.14 shows the U versus different q with various turbulator and error bar shows the standard deviation.

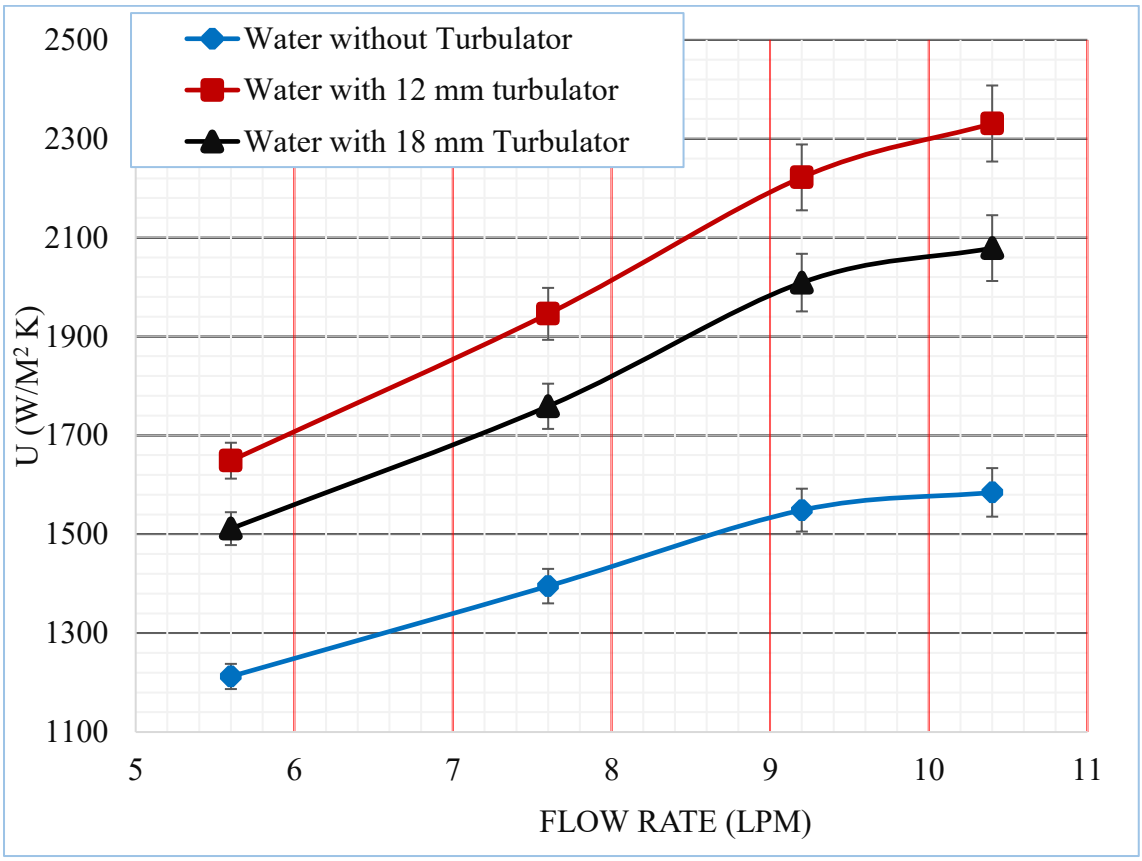

Figure 4. 14: U vs various turbulators for distilled water

4.7 Comparison of Overall heat transfer coefficient (U) with various turbulators for CuO-water nanofluid

Overall heat transfer coefficients for 18 mm turbulator and 12 mm turbulator increased by 25.42 % to 33.19 %; 37.49 % to 51.01 % respectively across flow rates ranging from 5.60 LPM to 10.4 LPM compare to CuO-water nanofluid without turbulator.

Figure 4.15 shows the U versus different q with different turbulator and error bar shows the standard deviation.

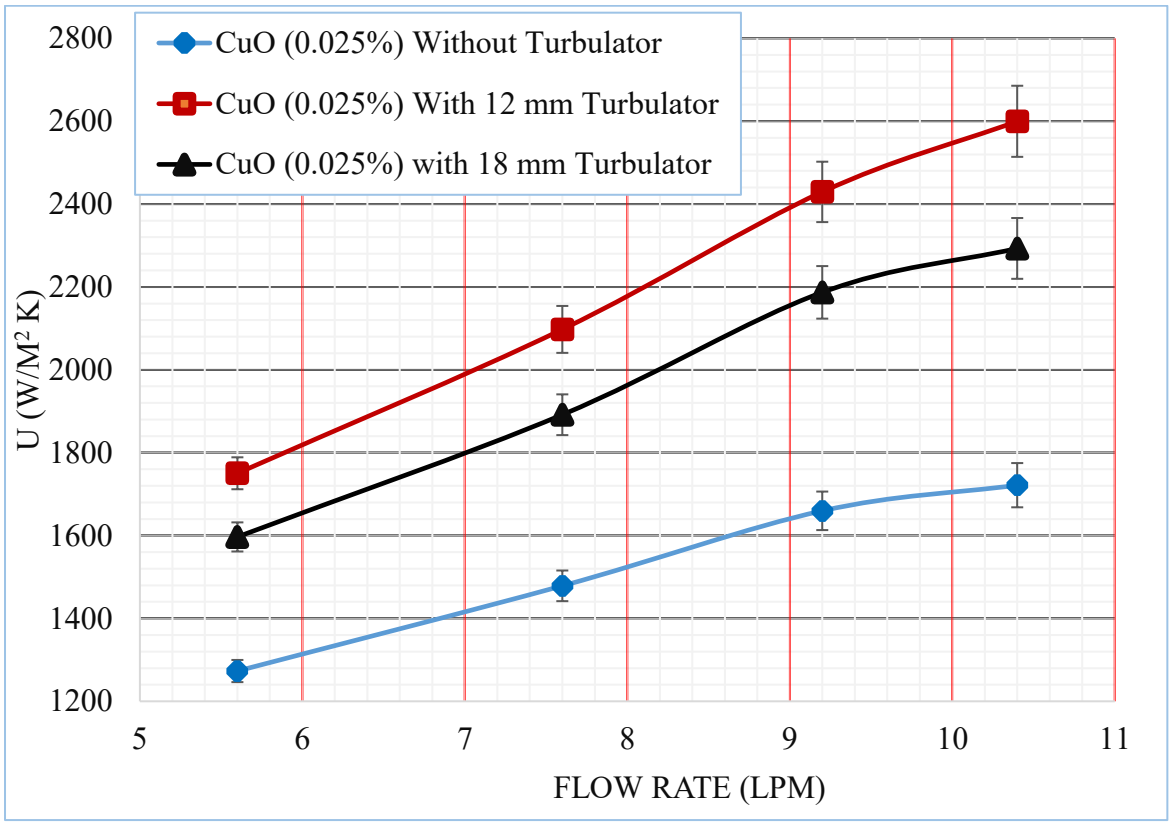

Figure 4. 15: U vs different turbulators for nanofluid

4.8 Comparison of Overall heat transfer coefficient (U) with various turbulators for CuO-Al_2O_3 (25:75) hybrid nanofluid

Overall heat transfer coefficients for 18 mm turbulator and 12 mm turbulator increased by 26.85 % to 36.41%; 38.43 % to 53.36% respectively across flow rates ranging from 5.60 LPM to 10.4 LPM compare to CuO-Al_2O_3 (25:75) hybrid nanofluid without turbulator.

Figure 4.16 shows the U versus different q with different turbulator and error bar shows the standard deviation.

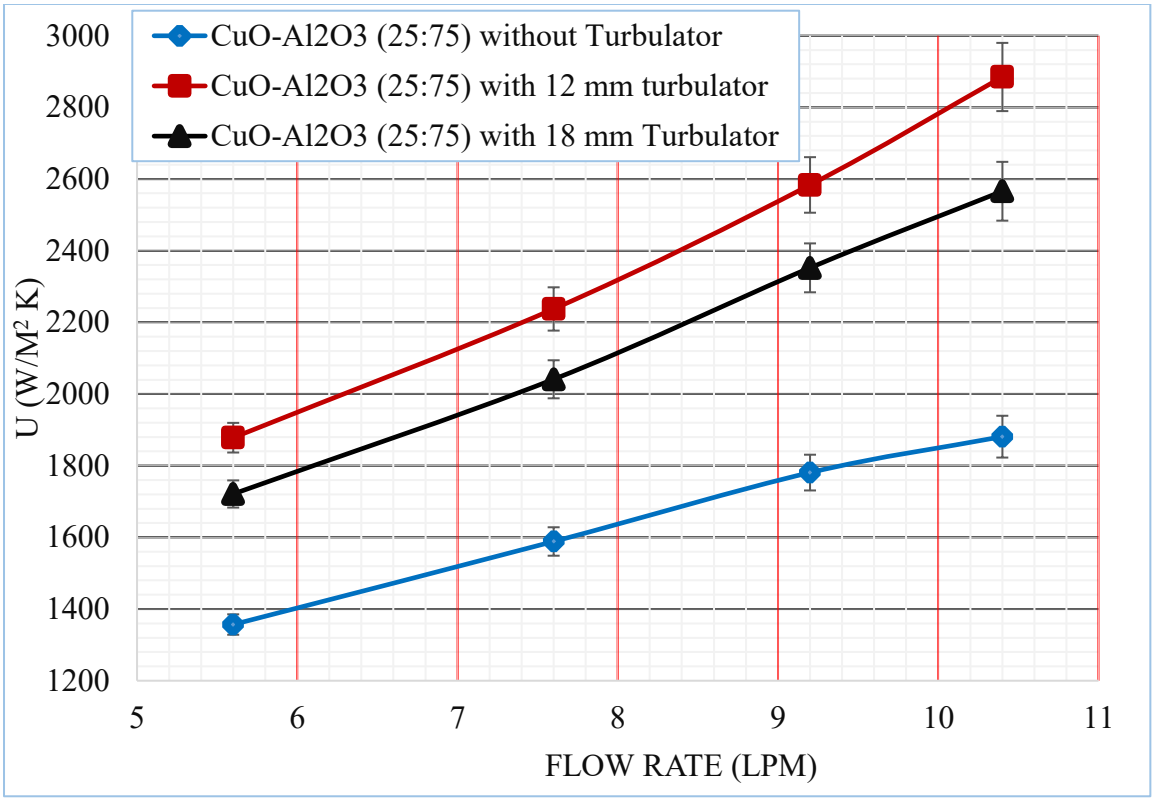

Figure 4. 16: U vs different turbulators for CuO-Al_2O_3 (25:75) hybrid nanofluid

4.9 Comparison of Overall heat transfer coefficient (U) with various turbulators for CuO-Al_2O_3 (50:50) hybrid nanofluid

Overall heat transfer coefficients for 18 mm turbulator and 12 mm turbulator increased by 31.32 % to 37.98%; 43.85 % to 55.64 % respectively across flow rates ranging from 5.60 LPM to 10.4 LPM compare to CuO-Al_2O_3 (50:50) hybrid nanofluid without turbulator.

Figure 4.17 shows the U versus different q with different turbulator and error bar shows the standard deviation.

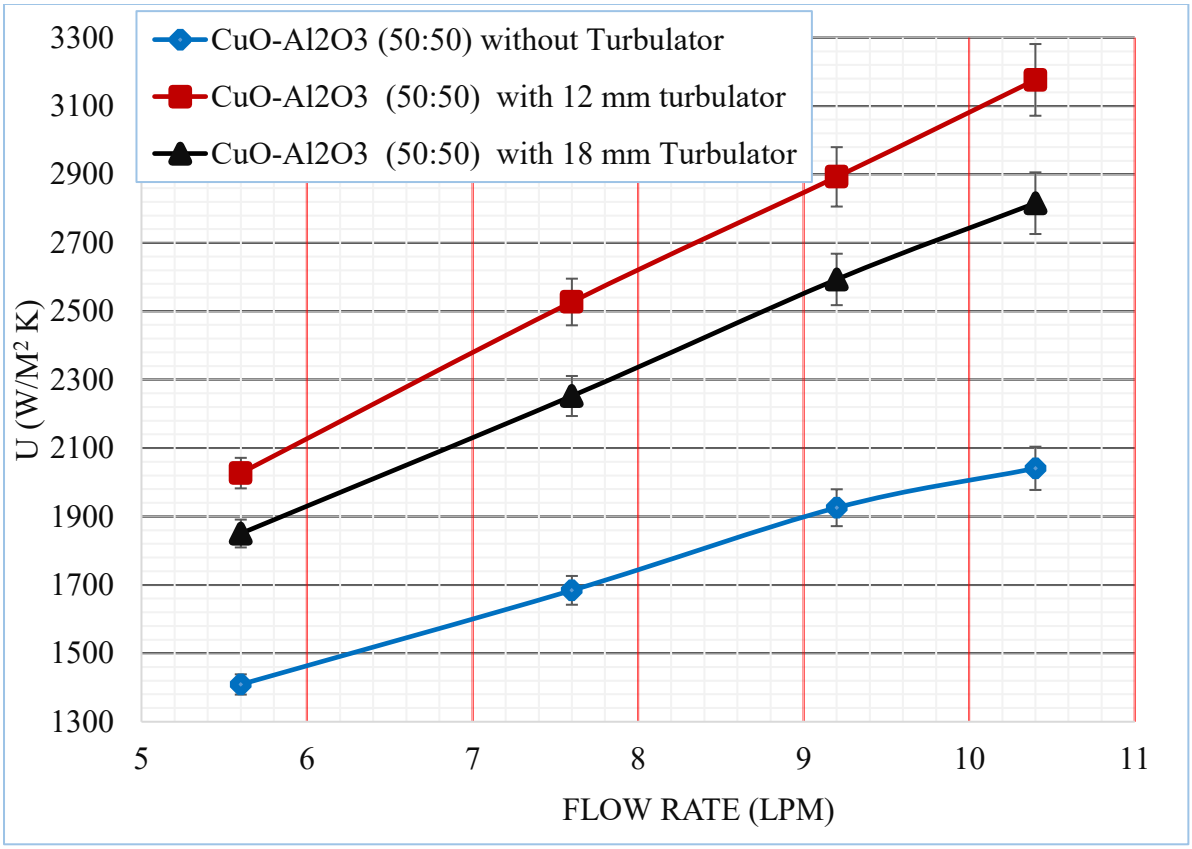

Figure 4. 17: U vs different turbulators for CuO-Al_2O_3 (50:50) hybrid nanofluid

4.10 Comparison of Overall heat transfer coefficient (U) with various turbulators for CuO-Al2O3 (75:25) hybrid nanofluid

Overall heat transfer coefficients for 18 mm turbulator and 12 mm turbulator increased by 35.43 % to 42.88 %; 48.90 % to 61.16 % across flow rates ranging from 5.60 LPM to 10.4 LPM compare to $CuO\text{-}Al_2O_3$ (75:25) hybrid nanofluid without turbulator.

Figure 4.18 shows the U versus different q with different turbulator and error bar shows the standard deviation.

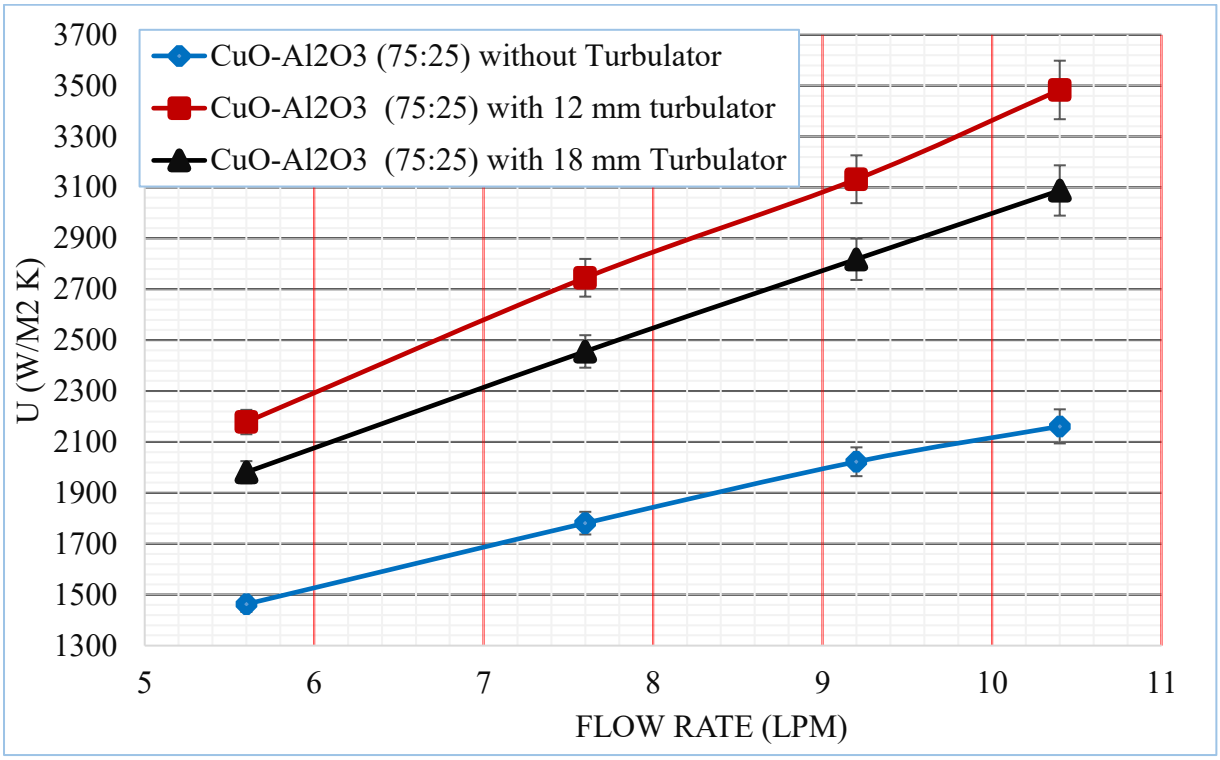

Figure 4. 18: U vs different turbulators for $CuO\text{-}Al_2O_3$ (75: 25) hybrid nanofluid

4.11 Comparison of pressure drop (ΔP) with various flow rate for various hybrid nanofluid proportion

After adding CuO nanoparticles and CuO-Al_2O_3 hybrid nanoparticles to the distilled water, pressure drop increased. Pressure drop for CuO (0.025%) nanofluid; CuO-Al_2O_3(25:75);CuO-Al_2O_3(50:50);CuO-Al_2O_3(75:25) hybrid nanofluids increased by 9.09 % to 20 % ;18.18 % to 36 %;27.2 % to 40 %; 36.3 % to 48 % across flow rates ranging from 5.60 LPM to 10.4 LPM compare to distilled water. According to Shabi et al.(2024) this rise in pressure drop results from a rise in viscosity and density because of nanoparticle concentration and increase in mass flow rates.

Figure 4.19 demonstrate the ΔP versus different q for distilled water and different hybrid nanofluid proportion and error bar shows the standard deviation.

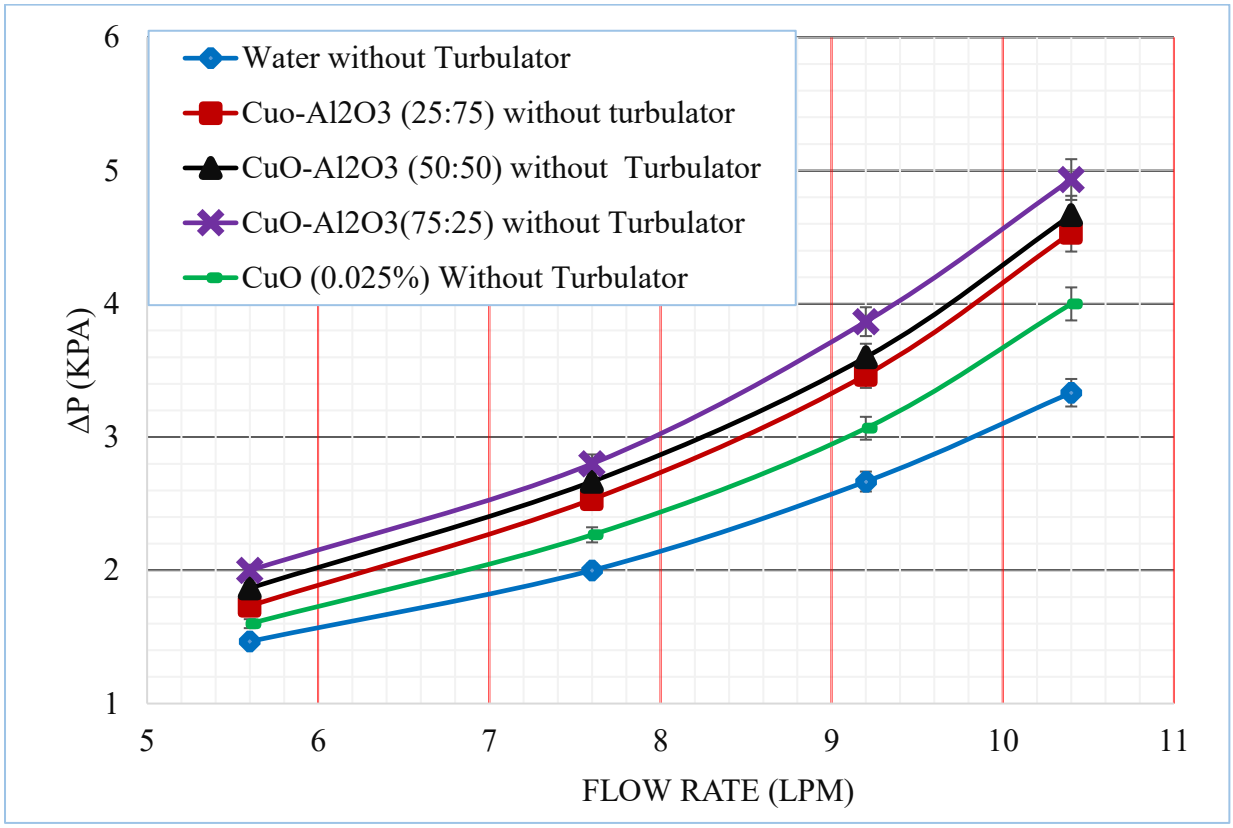

Figure 4. 19: ΔP vs various q for different hybrid nanofluid proportion

4.12 Comparison of pressure drop (ΔP) with 18 mm turbulators for various hybrid nanofluid proportion

Pressure drop for CuO (0.025%) nanofluid; CuO-Al2O3(25:75);CuO-Al2O3(50:50);CuO-Al2O3(75:25) hybrid nanofluids increased by 11.11 % to 20.61 %; 22.2 % to 39.3 %;33.3 % to 55.15 %; 46.47 % to 69.09 % across flow rates ranging from 5.60 LPM to 10.4 LPM with 18 mm pitch turbulator compare to distilled water.

Figure 4.20 shows the ΔP versus different q with 18 mm turbulator and error bar shows the standard deviation.

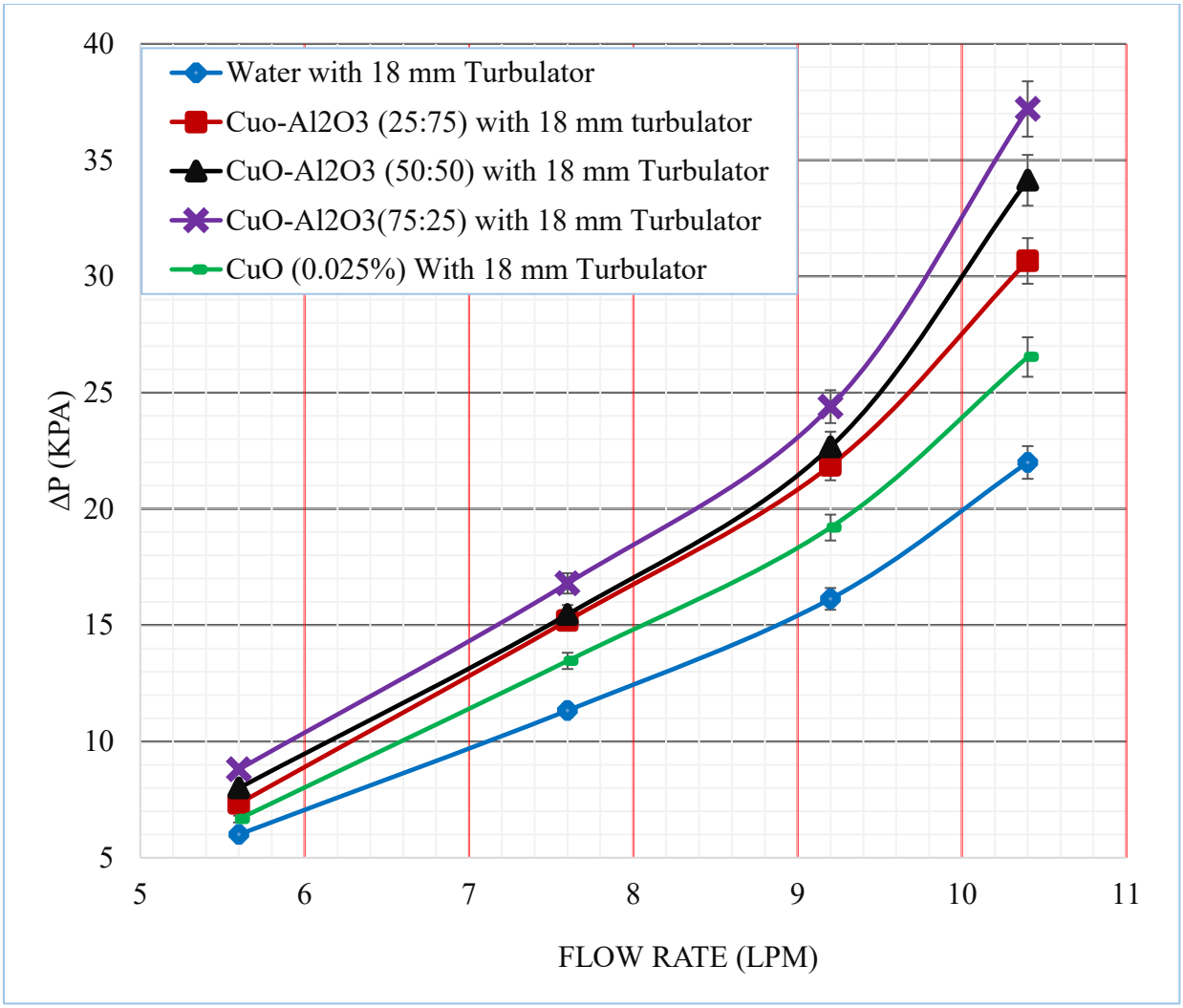

Figure 4. 20: ΔP vs different q with 18 mm turbulator

4.13 Comparison of pressure drop (ΔP) with 12 mm turbulators for various hybrid nanofluid proportion

Pressure drop for CuO (0.025%) nanofluid;CuO-Al2O3(25:75);CuO-Al2O3(50:50);CuO-Al2O3(75:25) hybrid nanofluids increased by 13.11% to 26.96%;31.15 % to 44.12 %; 47.54 % to 58.82 %; 65.57 % to 75.49 % across flow rates ranging from 5.60 LPM to 10.4 LPM with 12 mm pitch turbulator compare to distilled water.

Figure 4.21 shows the ΔP versus different q with 12 mm turbulator and error bar shows the standard deviation.

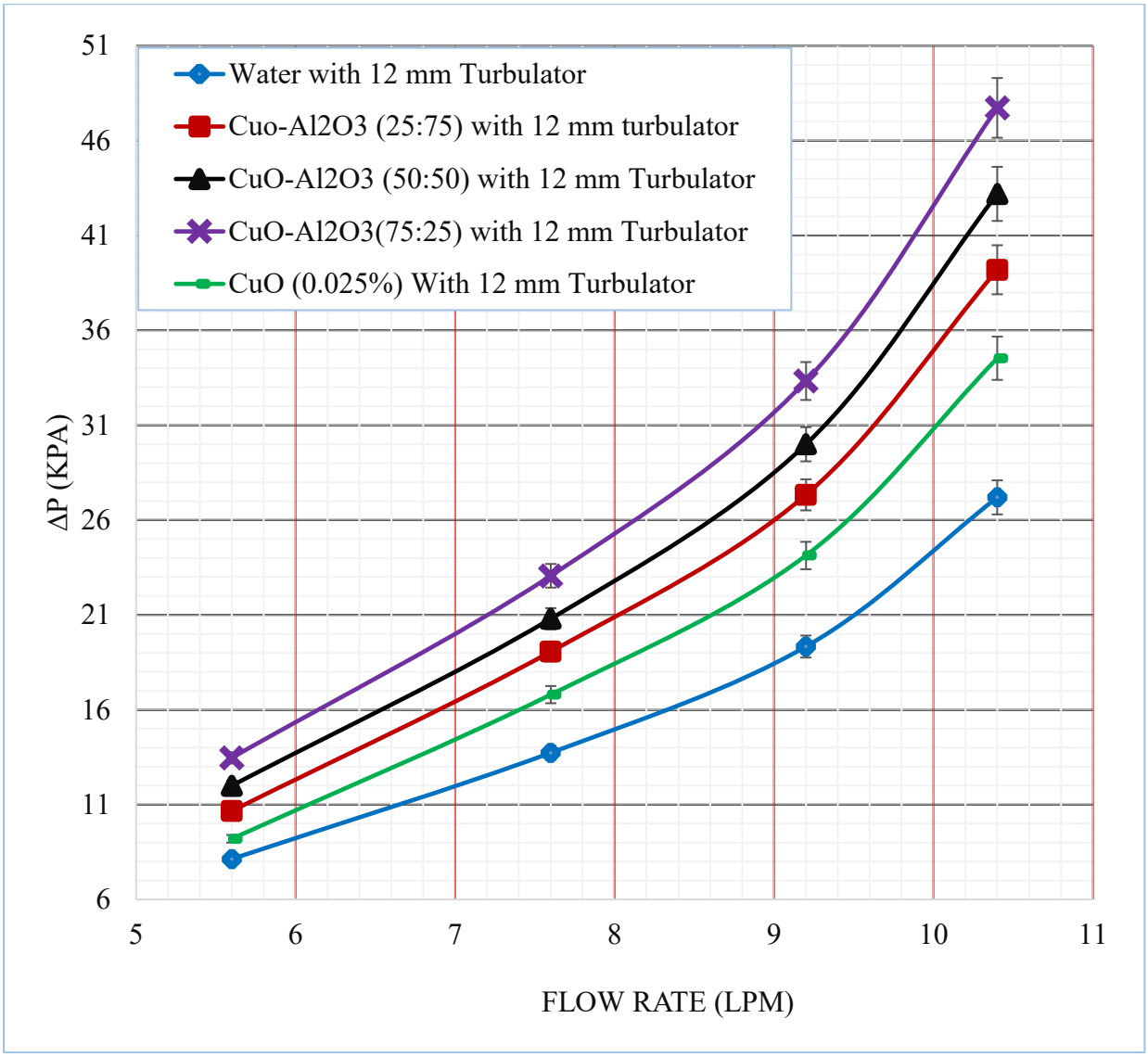

Figure 4. 21: ΔP vs different q with 12 mm turbulator

4.14 Comparison of pressure drop (ΔP) with various turbulators for distilled water

Adding 18 mm pitch helical coil turbulator, Pressure drop increased by 309.09 % to 560 %; across flow rates ranging from 5.60 LPM to 10.4 LPM compare to distilled water without turbulator. Replacing 18 mm pitch with smaller pitch turbulator which is 12 mm, Pressure drop increased by 454.55 % to 716 % across flow rates ranging from 5.60 LPM to 10.4 LPM compare to distilled water without turbulator. Lower pitch turbulator create more turbulence leading to more pressure drop.

Figure 4.22 displays the ΔP in relation to various q with different turbulators and error bar shows the standard deviation.

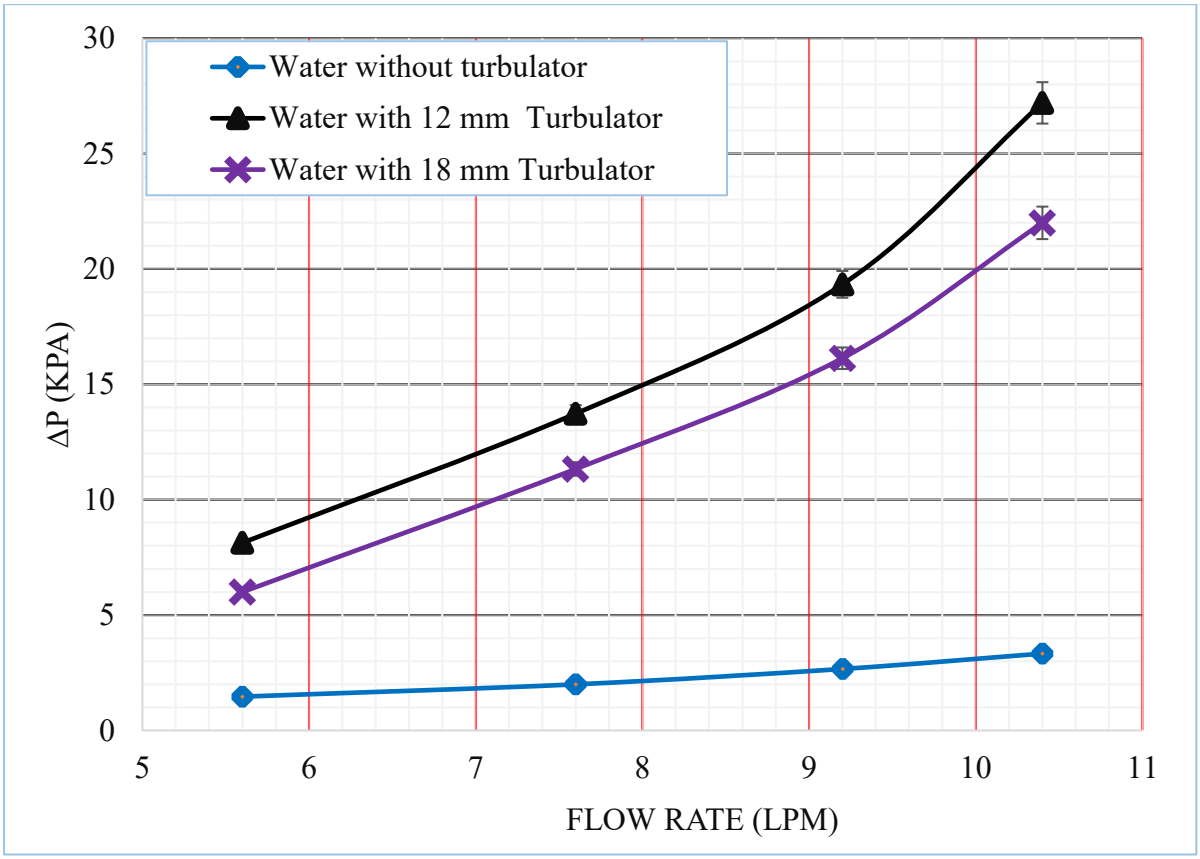

Figure 4. 22: ΔP vs different turbulators for distilled water

4.15 Comparison of pressure drop (ΔP) with various turbulators for CuO nanofluid

Pressure drop for 18 mm turbulator and 12 mm turbulator increased by 316.67 % to 563.33%; 475% to 763.33 % across flow rates ranging from 5.60 LPM to 10.4 LPM compare to CuO-water nanofluid without turbulator.

Figure 4.23 shows the ΔP versus different q with different turbulator and error bar shows the standard deviation.

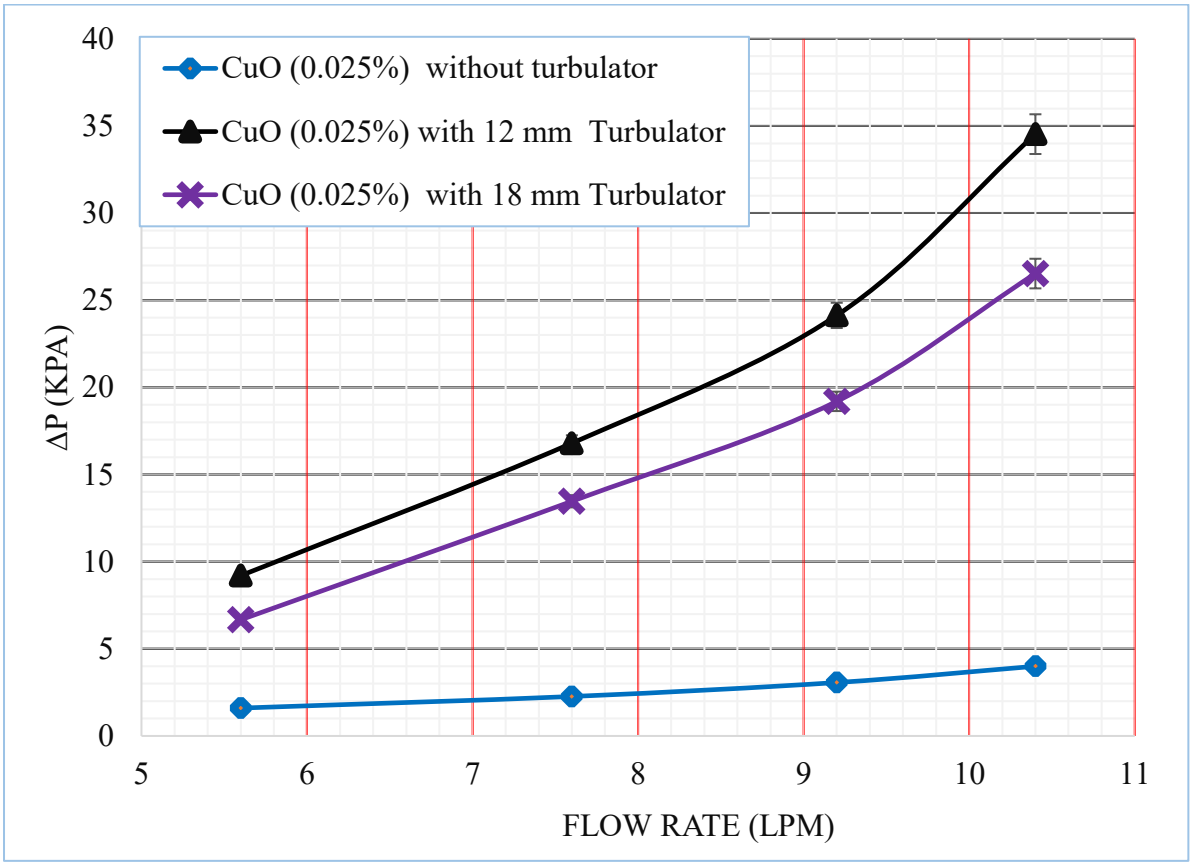

Figure 4. 23: ΔP vs different turbulators for CuO nanofluid

4.16 Comparison of pressure drop (ΔP) with various turbulators for CuO-Al_2O_3 (25:75) hybrid nanofluid

Pressure drop for 18 mm turbulator and 12 mm turbulator increased by 323.08 % to 576.47%; 515.38 % to 764.71 % across flow rates ranging from 5.60 LPM to 10.4 LPM compare to CuO-Al_2O_3 (25:75) hybrid nanofluid without turbulator.

Figure 4.22 shows the ΔP versus different q with different turbulator and error bar shows the standard deviation.

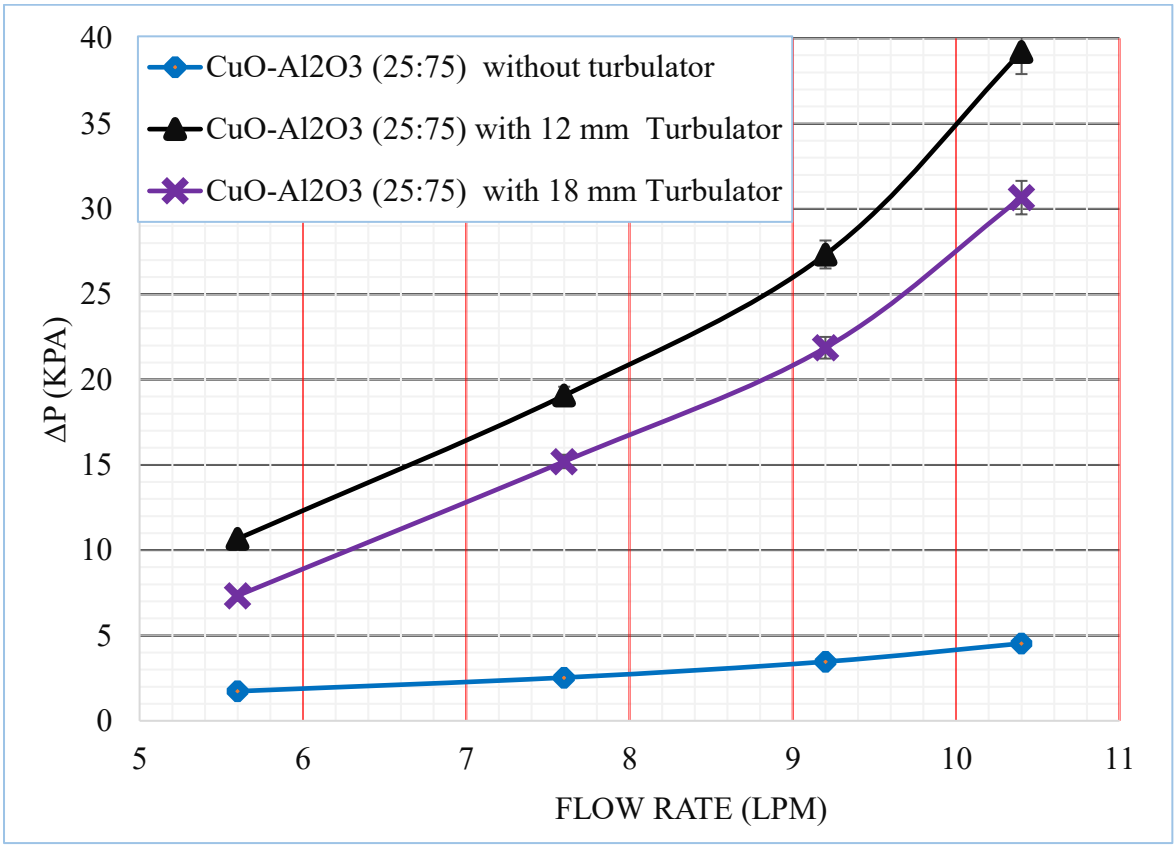

Figure 4. 24: ΔP vs different turbulators for CuO-Al_2O_3 (25:75) hybrid nanofluid

4.17 Comparison of pressure drop (ΔP) with various turbulators for CuO-Al_2O_3 (50:50) hybrid nanofluid

Pressure drop for 18 mm turbulator and 12 mm turbulator increased by 328.57 % to 631.43 %; 542.86 % to 825.71 % across flow rates ranging from 5.60 LPM to 10.4 LPM compare to CuO-Al_2O_3 (50:50) hybrid nanofluid without turbulator.

Figure 4.25 shows the ΔP versus different q with different turbulator and error bar shows the standard deviation.

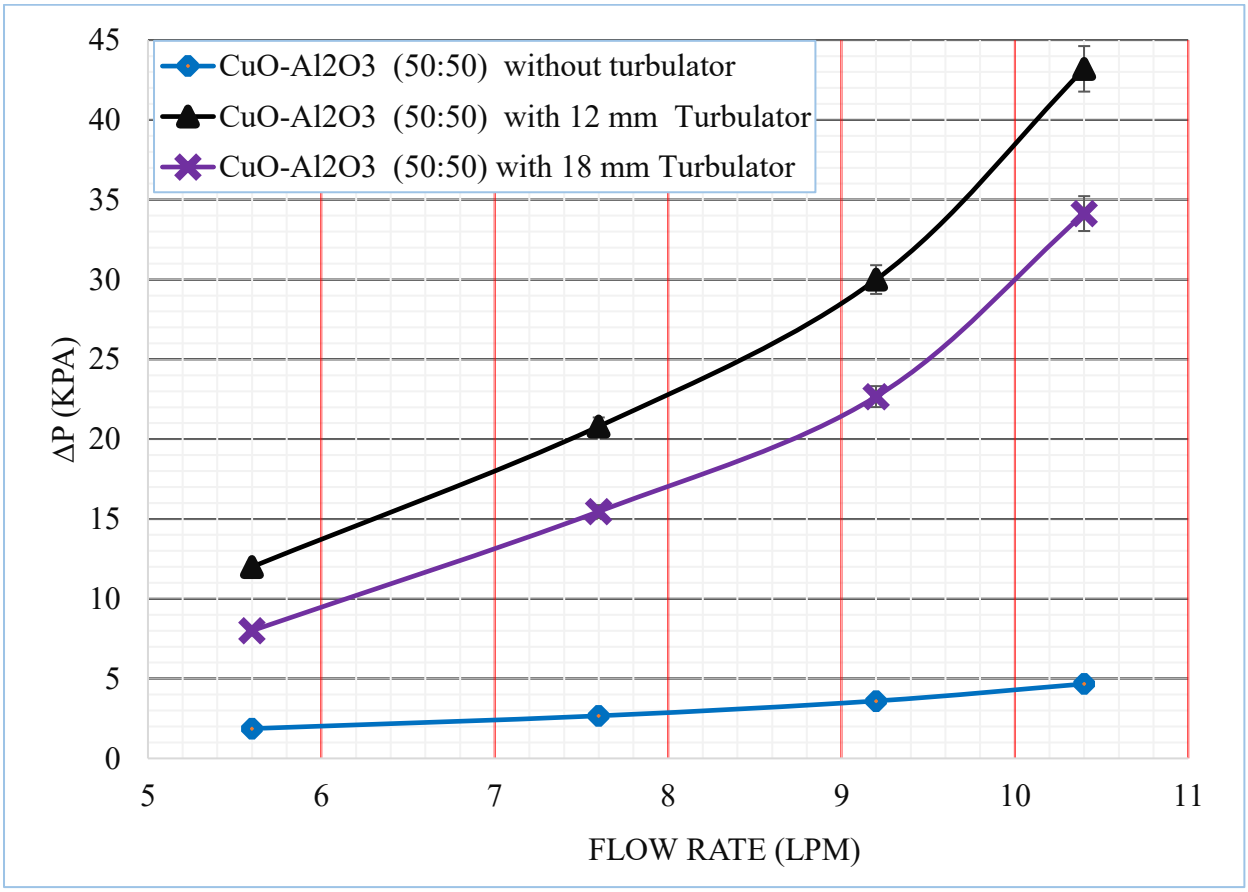

Figure 4. 25: ΔP vs different turbulators for CuO-Al_2O_3 (50: 50) hybrid nanofluid

4.18 Comparison of pressure drop (ΔP) with various turbulators for CuO-Al_2O_3 (75:25) hybrid nanofluid

Pressure drop for 18 mm turbulator and 12 mm turbulator increased by 340 % to 654.05 %; 573.33 % to 867.57 % across flow rates ranging from 5.60 LPM to 10.4 LPM compare to CuO-Al_2O_3 (75:25) hybrid nanofluid without turbulator.

Figure 4.26 shows the ΔP versus different q with different turbulator and error bar shows the standard deviation.

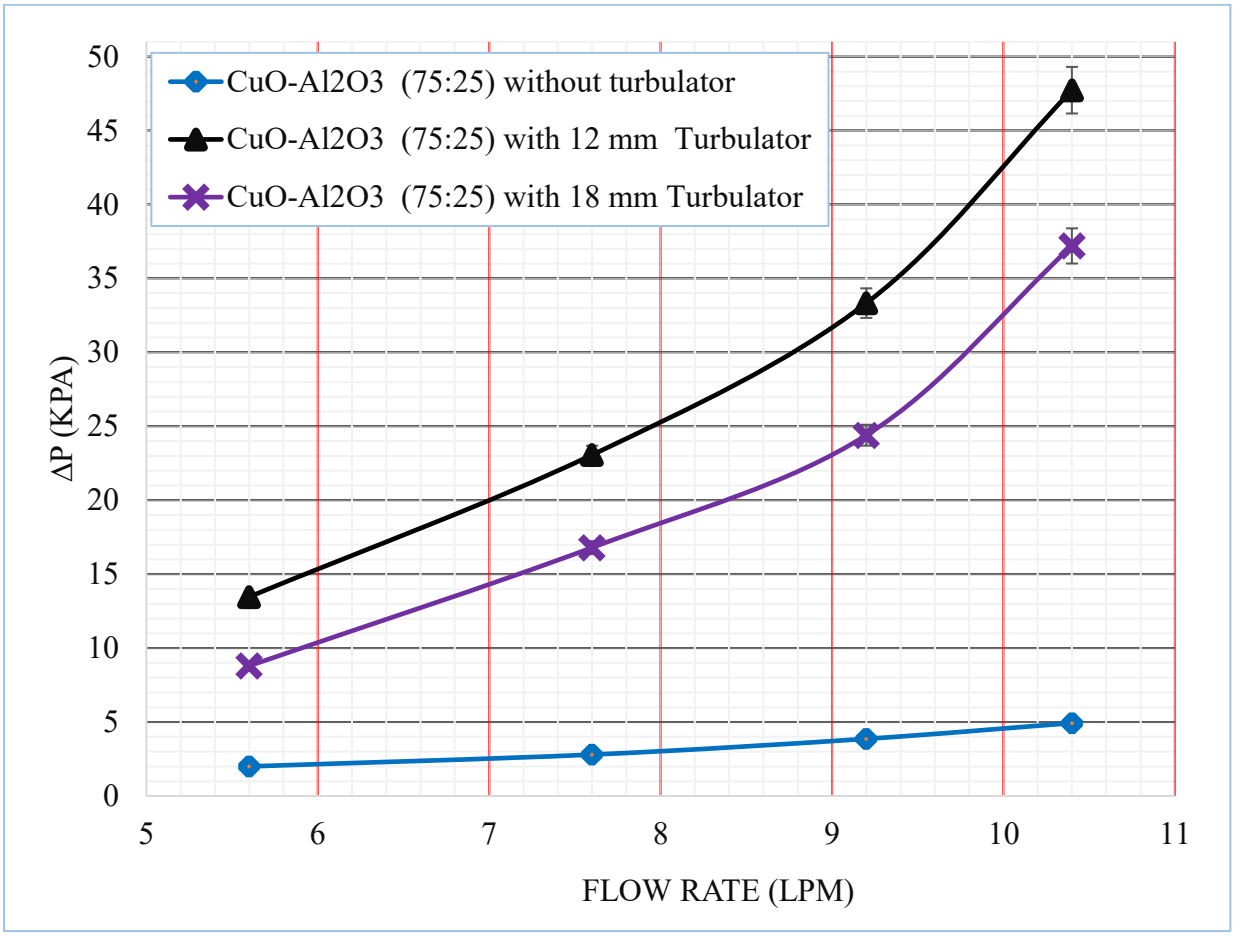

Figure 4. 26: ΔP vs different turbulators for CuO-Al_2O_3 (75: 25) hybrid nanofluid

CHAPTER FIVE: CONCLUSIONS AND RECOMMENDATIONS

5.1 Conclusions

Overall heat transfer coefficient and pressure drop were investigated using 12mm and 18 mm pitch helical coil turbulator along with CuO-water nanofluids, CuO-Al_2O_3-water hybrid nanofluids on counter flow concentric heat exchanger. The study explores CuO-water nanofluids with a volume concentration of 0.025% and hybrid nanoparticle concentrations of 0.1 % by volume and three proportions of CuO- Al_2O_3 (25:75,50:50 and 75:25) aiming to increase efficiency of concentric heat exchangers, energy consumption reduction and improve characteristics of conventional fluids. Experimental results indicate marked improvements in the overall heat transfer coefficient from the addition of CuO nanoparticles , CuO-Al_2O_3 hybrid nanoparticles, and a turbulator in distilled water. The study shows that helical coil turbulator with smaller pitch size intensify turbulence which in turn enhanced heat transfer. In expense of heat transfer adding nanoparticles in distilled water and turbulator in tube increased the pressure drop.

The experimental study shows that the overall heat transfer coefficients and pressure drop increases with increasing the flow rate. The overall heat transfer coefficients for distilled water without turbulator increased by 30.71 % and pressure drop increased by 127.27 % when flow rate increased from 5.60 LPM to 10.4 LPM.

The study shows that the helical coil turbulator with 12 mm pitch enhanced more heat transfer and increased more pressure drop than 18 mm pitch turbulator in distilled water and nanofluids. Overall heat transfer coefficients for 18 mm turbulator and 12 mm turbulator increased by 24.66 % to 31.18%; 36 % to 47.08 % and pressure drop increased by 309.09 % to 560%; 454.55 % to 716 % across flow rates ranging from 5.60 LPM to 10.4 LPM compare to distilled water without turbulator.

Overall heat transfer coefficients for CuO-nanofluid is increased by 5 % to 8.64 % and pressure drop increased by 9.09 % to 20 % across flow rates ranging from 5.60 LPM to 10.4 LPM compare to distilled water.

The study shows that maximum overall heat transfer coefficients enhancement and increase in pressure drop is for CuO-Al_2O_3 (75:25) hybrid nanofluids and for turbulator with 12 mm pitch. Overall heat transfer coefficients for CuO-Al_2O_3 (75:25) hybrid nanofluids increased by 20.67 % to 36.39 % and pressure drop increased by 36.3 % to 48 % across flow rates ranging from 5.60 LPM to 10.4 LPM compare to distilled water

without turbulator. Overall heat transfer coefficients of CuO-Al2O3 (75:25) hybrid nanofluid for 18 mm and 12 mm turbulator increased by 42.88 % and 61.16 % respectively and pressure drop increased by 654.05 % and 867.57 % respectively for flow rates 10.4 LPM compare to CuO-Al_2O_3 (75:25) hybrid nanofluid without turbulator.

5.2 Recommendations

The recommendation for additional research in this area are as follows:

- Determine how large range of hybrid nanoparticle concentrations affect pressure loss and heat transfer efficiency.
- Improve nanofluid performance by experimenting with other types of nanoparticles.
- Test various geometries and configurations of turbulated tubes to determine optimal designs.
- Evaluate the advantages and limitations of using hybrid nanofluids with turbulated tubes for various application.
- Performance Evaluation Criterion (PEC) can be conducted
- CFD modelling could be enhanced by including advanced turbulence models for more accurate simulation of flow behaviour .

REFERENCES

Akyürek, E. F., Geliş, K., Şahin, B., & Manay, E. (2018). Experimental analysis for heat transfer of nanofluid with wire coil turbulators in a concentric tube heat exchanger. *Results in Physics*, *9*, 376–389. https://doi.org/10.1016/j.rinp.2018.02.067

Alkam, M. K., & Al-Nimr, M. A. (1999). Improving the performance of double-pipe heat exchangers by using porous substrates. *International Journal of Heat and Mass Transfer*, *42*(19), 3609–3618. https://doi.org/10.1016/S0017-9310(99)00033-2

Alosious, S., R, S. S., Nair, A. R., & Krishnakumar, K. (2017). Experimental and numerical study on heat transfer enhancement of flat tube radiator using Al2O3 and CuO nanofluids. *Heat and Mass Transfer*, *53*(12), 3545–3563. https://doi.org/10.1007/s00231-017-2061-0

Awais, M., Bhuiyan, A. A., Salehin, S., Ehsan, M. M., Khan, B., & Rahman, M. H. (2021). Synthesis, heat transport mechanisms and thermophysical properties of nanofluids: A critical overview. *International Journal of Thermofluids*, *10*, 100086. https://doi.org/10.1016/j.ijft.2021.100086

Azmi, W. H., Sharma, K. V., Sarma, P. K., Mamat, R., & Najafi, G. (2014). Heat transfer and friction factor of water based TiO2 and SiO2 nanofluids under turbulent flow in a tube. *International Communications in Heat and Mass Transfer*, *59*, 30–38. https://doi.org/10.1016/j.icheatmasstransfer.2014.10.007

Bokov, D., Al-Attabi, A., Chupradit, S., Suksatan, W., Ansari, M., Shewael, I., & Valiev, G. (2021). Nanomaterial by Sol-Gel Method: Synthesis and Application. *Advances in Materials Science and Engineering*.

Çelik, H. S., & Erbay, L. B. (2021). Heat transfer enhancement using different types of turbulators on the heat exchangers. *Journal of Thermal Engineering*, *7*(7), 1654–1670. https://doi.org/10.18186/thermal.1025921

Eckert, E. R. G., & Drake, R. M. (1987). *Analysis of heat and mass transfer. Hemisphere*.

Fares, M., AL-Mayyahi, M., & AL-Saad, M. (2020). Heat transfer analysis of a shell and tube heat exchanger operated with graphene nanofluids. *Case Studies in Thermal Engineering*, *18*, 100584. https://doi.org/10.1016/j.csite.2020.100584

Ghashim, S. L. (2021). A mathematical analysis of nanoparticles on heat transfer in a circular pipe. *Case Studies in Thermal Engineering*, *28*, 101524. https://doi.org/10.1016/j.csite.2021.101524

Hassaan, A. M. (2024). An experimental investigation examining the usage of a hybrid nanofluid in an automobile radiator. *Scientific Reports*, *14*(1), 27597. https://doi.org/10.1038/s41598-024-78631-9

Ho, C. J., Huang, J. B., Tsai, P. S., & Yang, Y. M. (2010). Preparation and properties of hybrid water-based suspension of Al2O3 nanoparticles and MEPCM particles as functional forced convection fluid. *International Communications in Heat and Mass Transfer*, *37*(5), 490–494. https://doi.org/10.1016/j.icheatmasstransfer.2009.12.007

Karakaya, H., & Durmuş, A. (2013). Heat transfer and exergy loss in conical spring turbulators. *International Journal of Heat and Mass Transfer*, *60*, 756–762. https://doi.org/10.1016/j.ijheatmasstransfer.2013.01.054

Krasniqi, D., Selimaj, R., Krasniqi, M., & Filkoski, R. (n.d.). *THERMAL DYNAMIC ANALYSIS OF PARALLEL AND COUNTER FLOW HEAT EXCHANGERS*.

Leap CFD Team. (2012). *Tips & tricks: Convergence and mesh independence study*.

Modi, K. V., Patel, P. R., & Patel, S. K. (2023). Applicability of mono-nanofluid and hybrid-nanofluid as a technique to improve the performance of solar still: A critical review. *Journal of Cleaner Production*, *387*, 135875. https://doi.org/10.1016/j.jclepro.2023.135875

Nalavade, S. P., Prabhune, C. L., & Sane, N. K. (2019). Effect of novel flow divider type turbulators on fluid flow and heat transfer. *Thermal Science and Engineering Progress*, *9*, 322–331. https://doi.org/10.1016/j.tsep.2018.12.004

Owolabi, J., & Ojadi, P. (n.d.). *SYNTHESIS, CHARACTERIZATION AND X-RAY DIFFRACTION ANALYSIS OF ALUMINUM OXIDE NANOMATERIALS*.

Pak, B. C., & Cho, Y. I. (1998). HYDRODYNAMIC AND HEAT TRANSFER STUDY OF DISPERSED FLUIDS WITH SUBMICRON METALLIC OXIDE PARTICLES. *Experimental Heat Transfer*, *11*(2), 151–170. https://doi.org/10.1080/08916159808946559

Pordanjani, A. H., Aghakhani, S., Afrand, M., Sharifpur, M., Meyer, J. P., Xu, H., Ali, H. M., Karimi, N., & Cheraghian, G. (2021). Nanofluids: Physical phenomena, applications in thermal systems and the environment effects- a critical review. *Journal of Cleaner Production*, *320*, 128573. https://doi.org/10.1016/j.jclepro.2021.128573

Promvonge, P. (2008). Thermal performance in circular tube fitted with coiled square wires. *Energy Conversion and Management*, *49*(5), 980–987. https://doi.org/10.1016/j.enconman.2007.10.005

Radhakrishnan, A. A., & Beena, B. B. (2014). Structural and Optical Absorption Analysis of CuO Nanoparticles. *Indian Journal of Advances in Chemical Science*.

Rajendra, P., Dr. Mallikarjun.C. Math, & Syed, S. (2016). Design of Heat Exchanger with Effectiveness Improvement Techniques by using Fins and Inserts. *International Journal of Engineering Research*, *5*(08).

Rathodiya, B., & Vishnoi, S. (2017). *PREPARATION METHODS FOR NANOFLUIDS AND THERE STABILITY*.

Sagadevan, S., Pal, K., & Chowdhury, Z. Z. (2017). Fabrication of CuO nanoparticles for structural, optical and dielectric analysis using chemical precipitation method. *Journal of Materials Science: Materials in Electronics*, *28*(17), 12591–12597. https://doi.org/10.1007/s10854-017-7083-3

Said, Z., Sundar, L. S., Tiwari, A. K., Ali, H. M., Sheikholeslami, M., Bellos, E., & Babar, H. (2022). Recent advances on the fundamental physical phenomena behind stability, dynamic motion, thermophysical properties, heat transport, applications, and challenges of nanofluids. *Physics Reports*, *946*, 1–94. https://doi.org/10.1016/j.physrep.2021.07.002

Shabi, O. A., Alhazmy, M., Negeed, E.-S. R., & Elzoghaly, K. O. (2024). Experimental investigation of shell and helical coiled heat exchanger with Al2O3 nano-fluid with wide range of particle concentration. *Frontiers in Mechanical Engineering*, *10*, 1386254. https://doi.org/10.3389/fmech.2024.1386254

Shah, Z., Jafaryar, M., Sheikholeslami, M., Ikramullah, & Kumam, P. (2021). Heat transfer intensification of nanomaterial with involve of swirl flow device concerning entropy generation. *Scientific Reports*, *11*(1), 12504. https://doi.org/10.1038/s41598-021-91806-y

Shahmohammadi, P., & Beiki, H. (2016). *A numerical investigation of γ-Al2O3-water nanofluids heat transfer and pressure drop in a shell and tube heat exchanger*.

Shaik, A. H., Chakraborty, S., Saboor, S., Kumar, K. R., Majumdar, A., Rizwan, M., Arıcı, M., & Chandan, M. R. (2024). Cu-Graphene water-based hybrid nanofluids: Synthesis, stability, thermophysical characterization, and figure of merit analysis. *Journal of Thermal Analysis and Calorimetry*, *149*(7), 2953–2968. https://doi.org/10.1007/s10973-023-12875-x

Shristi Shefali Saraugi. (2024). *X-Ray Diffraction (XRD)-Basic principle, instrumentation, sample preparation, XRD plots, applications of XRD, XRD sample based errors*. https://doi.org/10.13140/RG.2.2.27075.82726

Vajjha, R. S., Das, D. K., & Namburu, P. K. (2010). Numerical study of fluid dynamic and heat transfer performance of Al2O3 and CuO nanofluids in the flat tubes of a radiator. *International Journal of Heat and Fluid Flow*, *31*(4), 613–621. https://doi.org/10.1016/j.ijheatfluidflow.2010.02.016

Vishnu Narayanan, M., & Rakesh, S. G. (2019). Analysis of heat transfer characteristics of nanofluid synthesized using green method. *IOP Conference Series: Materials Science and Engineering*, *577*(1), 012181. https://doi.org/10.1088/1757-899X/577/1/012181

Wanatasanappan, V. V., Abdullah, M. Z., & Gunnasegaran, P. (2020). Thermophysical properties of Al2O3-CuO hybrid nanofluid at different nanoparticle mixture ratio: An experimental approach. *Journal of Molecular Liquids*, *313*, 113458. https://doi.org/10.1016/j.molliq.2020.113458

Wollele, M. B., H.V, H., & Assaye, M. (2022). Heat transfer augmentation of $Al_2 O_3$ - Cu/water hybrid nanofluid in circular duct with inserts. *Cogent Engineering*, *9*(1), 2146627. https://doi.org/10.1080/23311916.2022.2146627

Xuan, Y., & Roetzel, W. (n.d.). *Conceptions for heat transfer correlation of nanoØuids*.

Zhang, S., Lu, L., Wen, T., & Dong, C. (2021). Turbulent heat transfer and flow analysis of hybrid Al2O3-CuO/water nanofluid: An experiment and CFD simulation study. *Applied Thermal Engineering*, *188*, 116589. https://doi.org/10.1016/j.applthermaleng.2021.116589

APPENDIX NO. 1 : EXPERIMENTAL SETUP AT THAPATHALI CAMPUS

Figure A1. 1: Experimental Setup

Figure A1. 2: Temperature Sensor

Figure A1. 3: Pressure Gauge

Figure A1. 4: Flow Sensor

Figure A1. 5: Hybrid Nanofluid during testing

APPENDIX NO. 2 : NANOFLUID PREPARATION AT PULCHOWK CAMPUS

Figure A2. 1: Muffle Furnace (left) and Ultrasonic Cleaner (Right)

Figure A2. 2: Gel-stage of Cuo (left) and Al_2O_3 (right)

Figure A2. 3: Hybrid Nanofluid

Figure A2. 4: Cuo-water Nanofluid preparation

APPENDIX NO. 3: SIMULATION SETUP

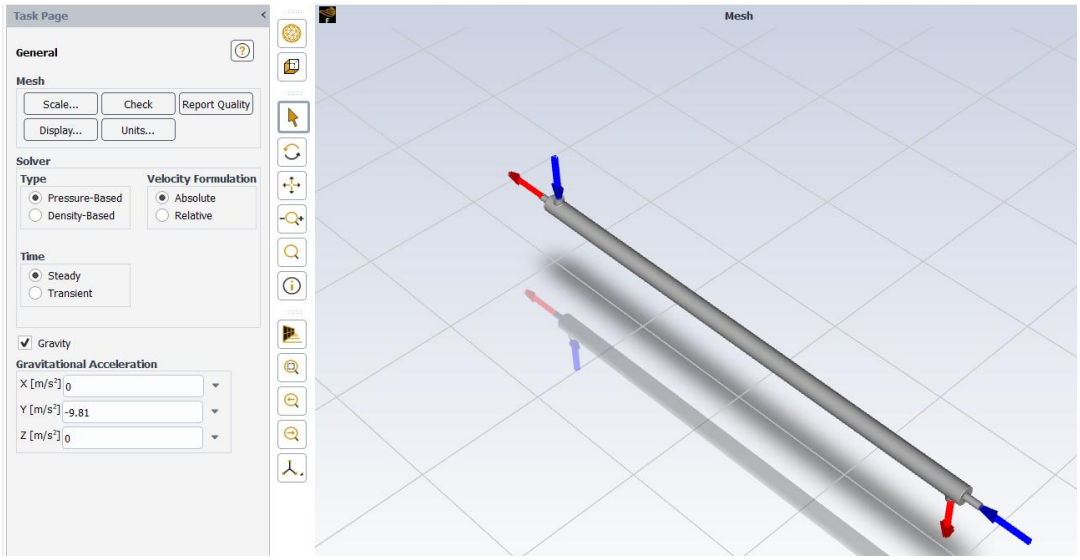

Figure A3. 1 simulation setup for the steady state simulation

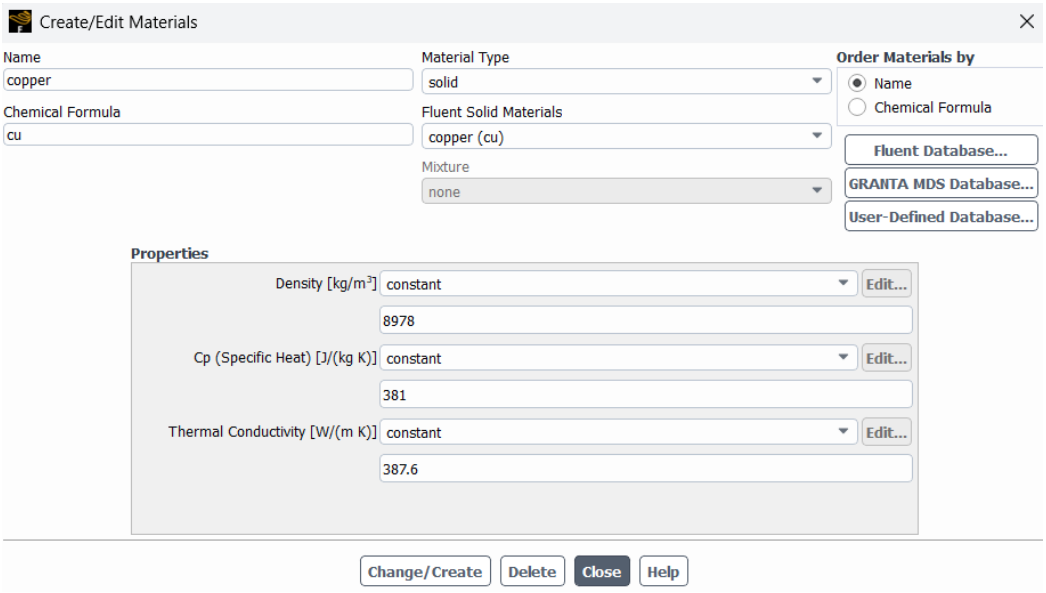

Figure A3. 2: Material properties of Copper Tube

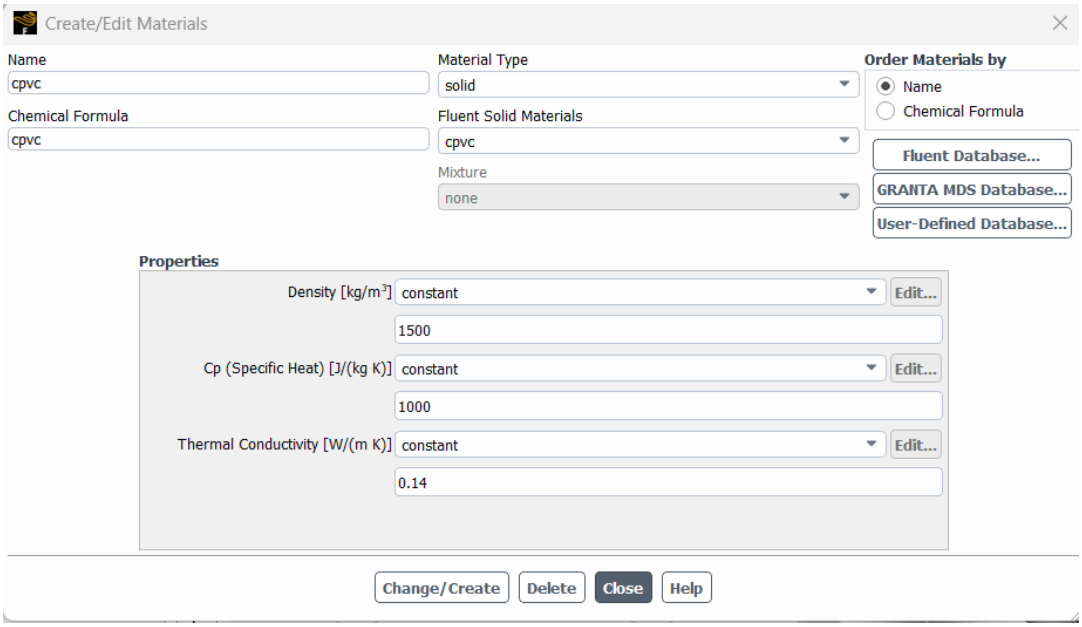

Figure A3. 3: Material Properties of CPVC Shell

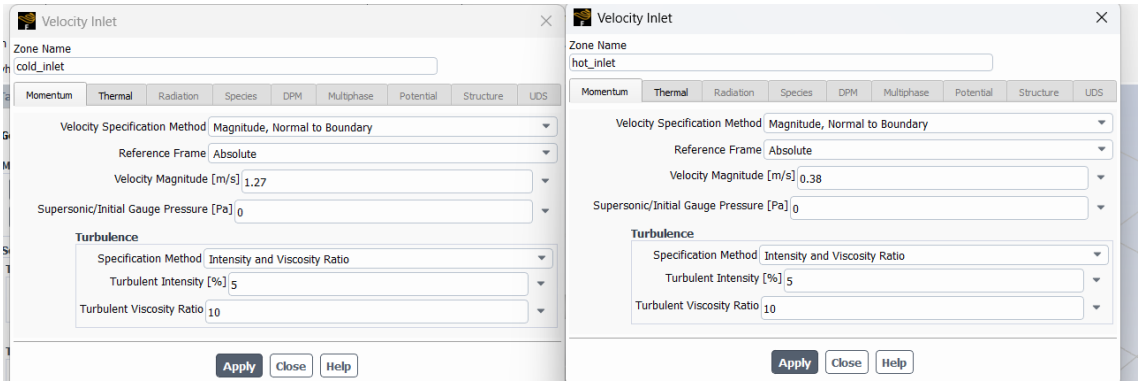

Figure A3. 4: Velocity Input

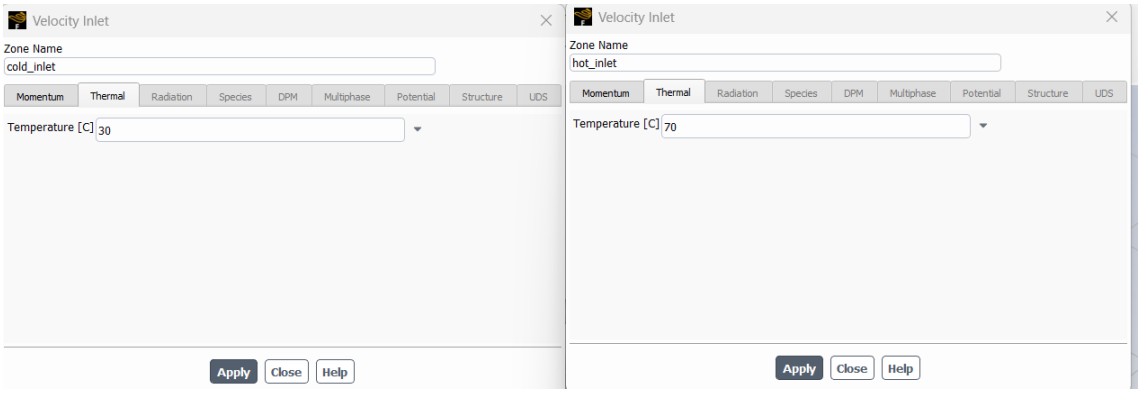

Figure A3. 5: Temperature Input

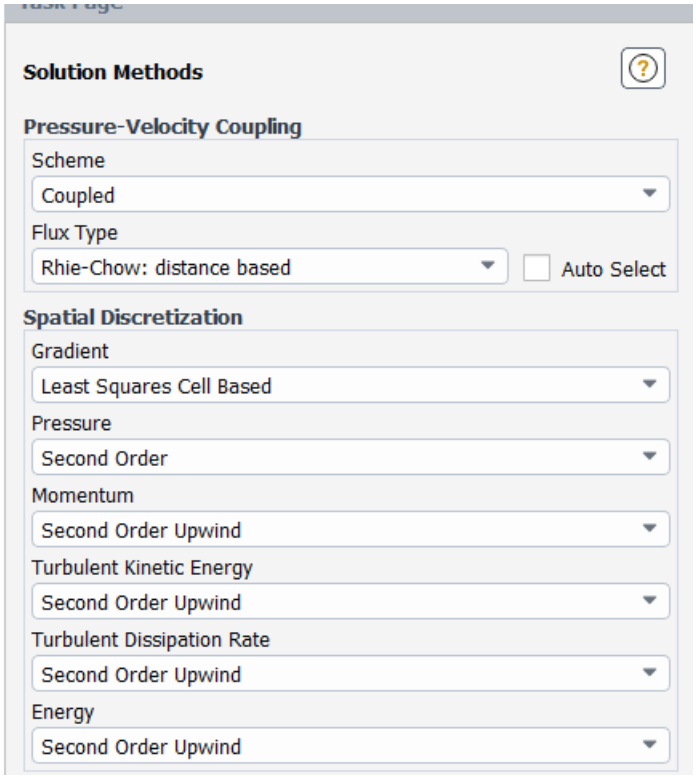

Figure A3. 6: Solution Method

APPENDIX NO. 4: EXPERIMENTAL DATA

Table A4. 1: For Distilled water without turbulator

For Pure water without turbulator							
Cold Fluid Flow (LPM)	Hot fluid Flow (LPM)	Tc1 (^{0}c)	Tc2 (^{0}c)	Th1 (^{0}c)	Th2 (^{0}c)	U (W/m^{2}K)	ΔP (kPa)
5.60	5.01	25	29.9	70	64.2	1212.40	1.47
7.60	5.01	25	29.4	70	63.7	1395.12	2.00
9.20	5.01	25	29	70	63	1548.81	2.67
10.40	5.01	25	28.3	70	62.2	1584.70	3.33

Table A4. 2: For CuO-Al_2O_3 (25:75) without turbulator

For CuO-Al_2O_3(25:75) without turbulator							
Cold Fluid Flow (LPM)	Hot fluid Flow (LPM)	Tc1 (^{0}c)	Tc2 (^{0}c)	Th1 (^{0}c)	Th2 (^{0}c)	U (W/m^{2}K)	ΔP (kPa)
5.60	5.01	25	30.5	70	63.7	1356.80	1.73
7.60	5.01	25	29.9	70	62.9	1588.53	2.53
9.20	5.01	25	29.4	70	61.9	1780.82	3.47
10.40	5.01	25	28.8	70	60.9	1881.06	4.53

Table A4. 3: For Al_2O_3 (50:50) without turbulator

For CuO-Al_2O_3(50:50) without turbulator							
Cold Fluid Flow (LPM)	Hot fluid Flow (LPM)	Tc1 (^{0}c)	Tc2 (^{0}c)	Th1 (^{0}c)	Th2 (^{0}c)	U (W/m^{2}K)	ΔP (kPa)
5.60	5.01	25	30.6	70	63.4	1408.98	1.87
7.60	5.01	25	30.2	70	62.6	1684.09	2.67
9.20	5.01	25	29.8	70	61.5	1925.67	3.60
10.40	5.01	25	29.1	70	60.3	2040.80	4.67

Table A4. 4: For CuO-Al_2O_3 (75:25) without turbulator

For CuO-Al_2O_3(75:25) without turbulator							
Cold Fluid Flow (LPM)	Hot fluid Flow (LPM)	Tc1 (^{0}c)	Tc2 (^{0}c)	Th1 (^{0}c)	Th2 (^{0}c)	U (W/m^{2}K)	ΔP (kPa)
5.60	5.01	25	30.8	70	63.2	1462.97	2.00
7.60	5.01	25	30.5	70	62.3	1781.16	2.80
9.20	5.01	25	30.1	70	61.3	2022.39	3.87
10.40	5.01	25	29.4	70	60	2161.38	4.93

Table A4. 5: For Pure water with 18 mm turbulator

For Pure water with 18 mm turbulator							
Cold Fluid Flow (LPM)	Hot fluid Flow (LPM)	Tc1 (^{0}c)	Tc2 (^{0}c)	Th1 (^{0}c)	Th2 (^{0}c)	U (W/m^{2}K)	ΔP (kPa)
5.60	5.01	25	30.5	70	62.5	1511.38	6.00
7.60	5.01	25	30.1	70	61.9	1758.84	11.33
9.20	5.01	25	29.8	70	60.9	2009.03	16.13
10.40	5.01	25	29.3	70	60.4	2078.79	22.00

Table A4. 6: For CuO- Al_2O_3(25:75) with 18 mm turbulator

For CuO-Al_2O_3(25:75) with 18 mm turbulator							
Cold Fluid Flow (LPM)	Hot fluid Flow (LPM)	Tc1 (^{0}c)	Tc2 (^{0}c)	Th1 (^{0}c)	Th2 (^{0}c)	U (W/m^{2}K)	ΔP (kPa)
5.60	5.01	25	31.3	70	61.8	1721.11	7.33
7.60	5.01	25	30.7	70	60.7	2041.16	15.20
9.20	5.01	25	30.4	70	59.5	2352.14	21.86
10.40	5.01	25	29.8	70	58	2565.86	30.66

Table A4. 7: For CuO- Al_2O_3 (50:50) with 18 mm turbulator

For CuO-Al_2O_3(50:50) with 18 mm turbulator							
Cold Fluid Flow (LPM)	Hot fluid Flow (LPM)	Tc1 (^{0}c)	Tc2 (^{0}c)	Th1 (^{0}c)	Th2 (^{0}c)	U (W/m^{2}K)	ΔP (kPa)
5.60	5.01	25	31.7	70	61.3	1850.23	8.00
7.60	5.01	25	31.1	70	59.8	2252.25	15.47
9.20	5.01	25	30.7	70	58.4	2593.01	22.66
10.40	5.01	25	30.3	70	57.3	2815.97	34.13

Table A4. 8: For CuO- Al_2O_3 (75:25) with 18 mm turbulator

For CuO-Al_2O_3(75:25) with 18 mm turbulator							
Cold Fluid Flow (LPM)	Hot fluid Flow (LPM)	Tc1 (^{0}c)	Tc2 (^{0}c)	Th1 (^{0}c)	Th2 (^{0}c)	U (W/m^{2}K)	ΔP (kPa)
5.60	5.01	25	32	70	60.7	1981.28	8.80
7.60	5.01	25	31.5	70	59	2455.83	16.80
9.20	5.01	25	30.9	70	57.3	2818.26	24.40
10.40	5.01	25	30.5	70	56	3088.27	37.20

Table A4. 9: For Pure water with 12 mm turbulator

For Pure water with 12 mm turbulator							
Cold Fluid Flow (LPM)	Hot fluid Flow (LPM)	Tc1 (^{0}c)	Tc2 (^{0}c)	Th1 (^{0}c)	Th2 (^{0}c)	U (W/m^{2}K)	ΔP (kPa)
5.60	5.01	25	30.9	70	61.9	1648.84	8.13
7.60	5.01	25	30.5	70	61.1	1945.80	13.73
9.20	5.01	25	30.1	70	59.9	2221.84	19.33
10.40	5.01	25	29.6	70	59.2	2330.84	27.20

Table A4. 10: For CuO- Al_2O_3 (25:75) with 12 mm turbulator

For CuO-Al_2O_3(25:75) with 12 mm turbulator							
Cold Fluid Flow (LPM)	Hot fluid Flow (LPM)	Tc1 (^{0}c)	Tc2 (^{0}c)	Th1 (^{0}c)	Th2 (^{0}c)	U (W/m^{2}K)	ΔP (kPa)
5.60	5.01	25	31.7	70	61.1	1864.14	10.67
7.60	5.01	25	31.1	70	59.9	2222.74	19.07
9.20	5.01	25	30.6	70	58.3	2567.99	27.33
10.40	5.01	25	30.2	70	56.7	2835.91	39.20

Table A4. 11: For CuO- Al_2O_3(50:50) with 12 mm turbulator

For CuO-Al_2O_3(50:50) with 12 mm turbulator							
Cold Fluid Flow (LPM)	Hot fluid Flow (LPM)	Tc1 (^{0}c)	Tc2 (^{0}c)	Th1 (^{0}c)	Th2 (^{0}c)	U (W/m^{2}K)	ΔP (kPa)
5.60	5.01	25	32.2	70	60.6	1969.43	12.00
7.60	5.01	25	31.4	70	58.4	2389.06	20.80
9.20	5.01	25	31	70	57	2779.28	30.00
10.40	5.01	25	30.8	70	56	3108.33	43.20

Table A4. 12: For CuO-Al_2O_3(75:25) with 12 mm turbulator

For CuO-Al_2O_3(75:25) with 12 mm turbulator							
Cold Fluid Flow (LPM)	Hot fluid Flow (LPM)	Tc1 (^{0}c)	Tc2 (^{0}c)	Th1 (^{0}c)	Th2 (^{0}c)	U (W/m^{2}K)	ΔP (kPa)
5.60	5.01	25	32.6	70	60	2163.55	13.47
7.60	5.01	25	31.6	70	57.3	2648.87	23.06
9.20	5.01	25	31.4	70	56.2	3047.57	33.33
10.40	5.01	25	31	70	54.6	3357.95	47.73

Table A4. 13: For CuO(0.025%)-water without turbulator

For CuO(0.025%)-water without turbulator							
Cold Fluid Flow (LPM)	Hot fluid Flow (LPM)	Tc1 (^{0}c)	Tc2 (^{0}c)	Th1 (^{0}c)	Th2 (^{0}c)	U (W/m^{2}K)	ΔP (kPa)
5.60	5.01	25	30.15	70	64	1273.05	1.60
7.60	5.01	25	29.57	70	63.3	1478.67	2.27
9.20	5.01	25	29.2	70	62.5	1659.70	3.07
10.40	5.01	25	28.5	70	61.55	1721.58	4.00

Table A4. 14: For CuO(0.025%)-water with 12 mm turbulator

For CuO(0.025%)-water with 12 mm turbulator							
Cold Fluid Flow (LPM)	Hot fluid Flow (LPM)	Tc1 (^{0}c)	Tc2 (^{0}c)	Th1 (^{0}c)	Th2 (^{0}c)	U (W/m^{2}K)	ΔP (kPa)
5.60	5.01	25	31.2	70	61.5	1750.32	9.20
7.60	5.01	25	30.75	70	60.4	2097.55	16.80
9.20	5.01	25	30.3	70	58.85	2429.42	24.13
10.40	5.01	25	29.85	70	57.9	2599.77	34.53

Table A4. 15: For CuO(0.025%)-water with 18 mm turbulator

For CuO(0.025%)-water with 18 mm turbulator							
Cold Fluid Flow (LPM)	Hot fluid Flow (LPM)	Tc1 (^{0}c)	Tc2 (^{0}c)	Th1 (^{0}c)	Th2 (^{0}c)	U (W/m^{2}K)	ΔP (kPa)
5.60	5.01	25	30.8	70	62.2	1596.71	6.67
7.60	5.01	25	30.35	70	61.3	1891.62	13.47
9.20	5.01	25	30	70	60	2186.94	19.20
10.40	5.01	25	29.5	70	59.3	2293.01	26.53

Gmail Parajuli Laxmi <parajulilaxmi400@gmail.com>

Revised Manuscript

TUTA Pashchimanchal Campus <journal.tuta@gmail.com> Fri, Nov 28, 2025 at 2:19 PM
To: Parajuli Laxmi <parajulilaxmi400@gmail.com>

Dear author(s),
We are pleased to inform you that your manuscript titled "Experimental Investigation of Thermal Enhancement Using CuO-Water Nanofluid in a Tube Equipped with Helical Turbulators" has been accepted after peer review for publication in the 9th Volume of Oodbodhan(ISSN 2091-2676) on 28th November 2025.

Regards,
Editorial Board
[Quoted text hidden]

Final Thesis Report_Laxmi Parajuli -II.pdf

Tribhuvan University

Document Details

Submission ID
trn:oid:::3117:540456687

Submission Date
Dec 14, 2025, 3:45 PM GMT+5:45

Download Date
Dec 14, 2025, 3:48 PM GMT+5:45

File Name
Final Thesis Report_Laxmi Parajuli -II.pdf

File Size
2.4 MB

70 Pages

14,430 Words

84,886 Characters

iThenticate Page 1 of 76 - Cover Page Submission ID trn:oid:::3117:540456687

5% Overall Similarity

The combined total of all matches, including overlapping sources, for each database.

Filtered from the Report

- Bibliography
- Quoted Text
- Cited Text
- Small Matches (less than 10 words)

Custom Section Exclusions

{titlesCount} Section Titles, {keywordsCount} Keywords

Section title	No. of Section Starters	Section Starters
"Acknowledgements"	4	Acknowledgements, Acknowledgement, Acknowledgment, Acknowledgments

Match Groups

- 50 Not Cited or Quoted 5%
  Matches with neither in-text citation nor quotation marks
- 0 Missing Quotations 0%
  Matches that are still very similar to source material
- 0 Missing Citation 0%
  Matches that have quotation marks, but no in-text citation
- 0 Cited and Quoted 0%
  Matches with in-text citation present, but no quotation marks

Top Sources

3% Internet sources
2% Publications
0% Submitted works (Student Papers)

Integrity Flags

1 Integrity Flag for Review

Replaced Characters
30 suspect characters on 9 pages
Letters are swapped with similar characters from another alphabet.

Our system's algorithms look deeply at a document for any inconsistencies that would set it apart from a normal submission. If we notice something strange, we flag it for you to review.

A Flag is not necessarily an indicator of a problem. However, we'd recommend you focus your attention there for further review.

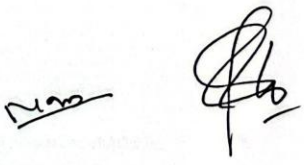

Match Groups

- 50 Not Cited or Quoted 5%
  Matches with neither in-text citation nor quotation marks
- 0 Missing Quotations 0%
  Matches that are still very similar to source material
- 0 Missing Citation 0%
  Matches that have quotation marks, but no in-text citation
- 0 Cited and Quoted 0%
  Matches with in-text citation present, but no quotation marks

Top Sources

3% Internet sources
2% Publications
0% Submitted works (Student Papers)

Top Sources

The sources with the highest number of matches within the submission. Overlapping sources will not be displayed.

1	Internet	
etd.aau.edu.et		<1%
2	Internet	
repository.sustech.edu		<1%
3	Publication	
Sobin Alosious, Sarath S R, Anjan R Nair, K Krishnakumar. "Experimental and num...		<1%
4	Internet	
www.coursehero.com		<1%
5	Internet	
www.thepharmajournal.com		<1%
6	Publication	
"Proceedings of Fluid Mechanics and Fluid Power (FMFP) 2023, Vol. 3", Springer Sc...		<1%
7	Publication	
A. E. Zohir, M. A. Habib, M. A. Nemitallah. "Heat Transfer Characteristics in a Doub...		<1%
8	Internet	
datapdf.com		<1%
9	Internet	
www.lib.umd.edu		<1%
10	Publication	
W.V. Vicki, M.Z. Abdullah, P. Gunnasegaran. "Thermophysical properties of Al2O3-...		<1%